SANDIA REPORT

SAND2003-1193
Unlimited Release
Printed April 2003

Experimental Investigations of an Inclined Lap-Type Bolted Joint

Danny L. Gregory, Brian R. Resor, Ronald G. Coleman, and David O. Smallwood

Prepared by
Sandia National Laboratories
Albuquerque, New Mexico 87185 and Livermore, California 94550

Sandia is a multiprogram laboratory operated by Sandia Corporation,
a Lockheed Martin Company, for the United States Department of Energy's
National Nuclear Security Administration under Contract DE-AC04-94AL85000.

Issued by Sandia National Laboratories, operated for the United States Department of Energy by Sandia Corporation.

Available to DOE and DOE contractors from
U.S. Department of Energy
Office of Scientific and Technical Information
P.O. Box 62
Oak Ridge, TN 37831

Telephone: (865)576-8401
Facsimile: (865)576-5728
E-Mail: reports@adonis.osti.gov
Online ordering: http://www.doe.gov/bridge

Available to the public from
U.S. Department of Commerce
National Technical Information Service
5285 Port Royal Rd
Springfield, VA 22161

Telephone: (800)553-6847
Facsimile: (703)605-6900
E-Mail: orders@ntis.fedworld.gov
Online order: http://www.ntis.gov/help/ordermethods.asp?loc=7-4-0#online

SAND2003-1193
Unlimited Release
Printed April 2003

Experimental Investigations of an Inclined Lap-Type Bolted Joint

Danny L. Gregory, Brian R. Resor, and Ronald G. Coleman
Advanced Diagnostics and Testing Department

David O. Smallwood
Structural Dynamics Research Department

Sandia National Laboratories
P.O. Box 5800
Albuquerque, NM 87185-0555

Abstract

The dynamic response of critical aerospace components is often strongly dependent upon the dynamic behavior of bolted connections that attach the component to the surrounding structure. These bolted connections often provide the only structural load paths to the component. The bolted joint investigated in this report is an inclined lap-type joint with the interface inclined with respect to the line of action of the force acting on the joint. The accurate analytical modeling of these bolted connections is critical to the prediction of the response of the component to normal and high-level shock environmental loadings. In particular, it is necessary to understand and correctly model the energy dissipation (damping) of the bolted joint that is a nonlinear function of the forces acting on the joint. Experiments were designed and performed to isolate the dynamics of a single bolted connection of the component. Steady state sinusoidal and transient experiments were used to derive energy dissipation curves as a function of input force. Multiple assemblies of the bolted connection were also observed to evaluate the variability of the energy dissipation of the connection. These experiments provide insight into the complex behavior of this bolted joint to assist in the postulation and development of reduced order joint models to capture the important physics of the joint including stiffness and damping. The experiments are described and results presented that provide a basis for candidate joint model calibration and comparison.

Acknowledgements

The authors would like to thank Dan Segalman for his invaluable insight and modeling support to assist the interpretation of the experimental results. The authors would also like to thank Tom Paez and Angel Urbina for their support with modeling and suggestions regarding uncertainty quantification. Thanks are also in order for the modeling efforts of Don Lobitz, Ron Hopkins, and Fernando Bitsie. The authors are also indebted to Mike Nusser for his innovative design and hardware support activities that span the entire joints research effort.

Table of Contents

Table of Figures

Introduction

The analytical modeling of bolted connections of a structural component to its mounting points is critical to the prediction of the response of the component to normal and high-level shock environmental loadings. These bolted connections often provide the only structural load paths to the component. In particular, it is necessary to understand and correctly model the energy dissipation (damping) of the bolted joint that is a nonlinear function of the forces acting on the joint. Experiments discussed in this report were designed to isolate a single bolted connection to focus the investigations to assist in the development of a reduced order model representing the energy dissipation of the connection. The bolted joint investigated is a lap-type joint with an interface inclined with respect to the line of action of the force. Multiple assemblies of the bolted joint were used to evaluate the variability of the energy dissipation of the connection. These experiments have been used to provide insight into the complex behavior of this bolted joint to assist in the postulation and development of candidate joint models [1,2,3] to capture the important physics of the joint including stiffness and damping.

Energy Dissipation Studies

A bolted connection of the component identified in the plots as the AF&F was initially studied by designing an experiment to investigate the behavior of a "single-leg" of a multi-legged attachment. Test specimens capturing the local geometry of the connection were fabricated as shown in Figure 1 and Figure 2. The same materials, titanium and stainless steel, used for the actual AF&F connection were used along with the same type of bolt used for the actual assembly. During observations of assembly of the component parts to the mounting hardware the vertical gap between the base of the component and the legs of the attachment hardware was observed to range from a few thousandth's of an inch to a light contact condition. This vertical gap is shown in an expanded view in Figure 3. Experiments were performed with a gap of 0.010 inch and with the gap closed to investigate the effect on the energy dissipation.

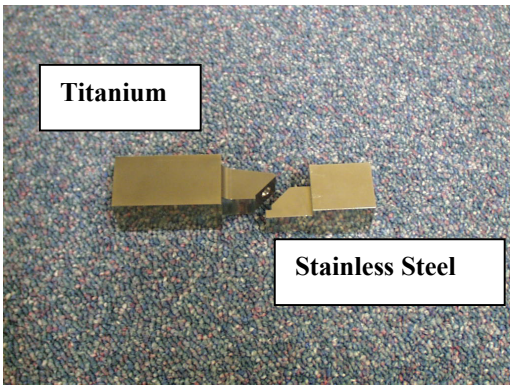

Figure 1. Single leg test specimen.

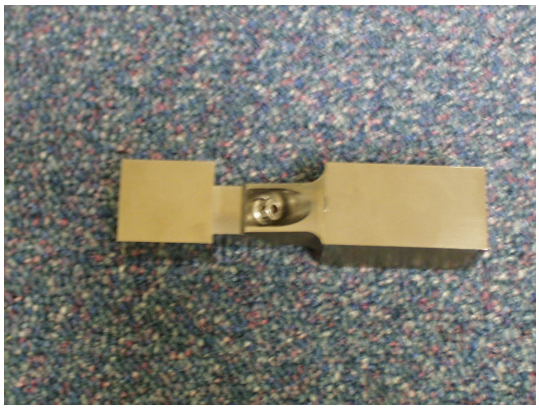

Figure 2. Single leg test specimen w/bolt.

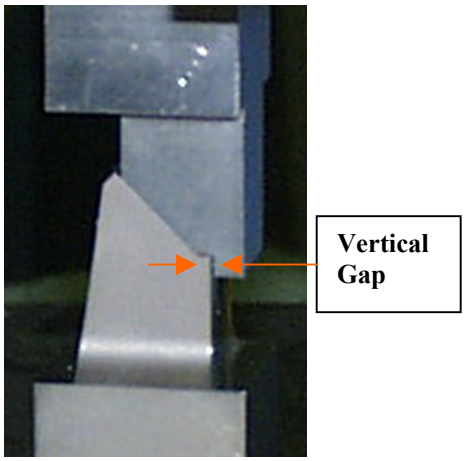

Figure 3. Expanded view of vertical gap.

The single-leg specimen was assembled into the microslip [4,5] experimental hardware to create a single degree of freedom (SDOF) system. The test specimen essentially represents a non-linear spring in the system. The large inertial mass is supported by soft springs to balance the static weight of the system. The experimental setup is shown in Figure 4. A piezoelectric force gage was used beneath the test specimen to measure the input force. Piezoelectric accelerometers were used to measure the accelerations of the base and the mass. The excitation for the experiments was provided with a T1000 Unholtz-Dickie electrodynamic exciter. A Spectral Dynamics 2552 Vibration Control System was used to generate and control the excitation waveforms used in the experiments. The response of the mass to base excitation is very sensitive to changes in the bolted joint. These changes can be associated with bolt torque and interface pressure, seating of the interfaces, wear, and other sources.

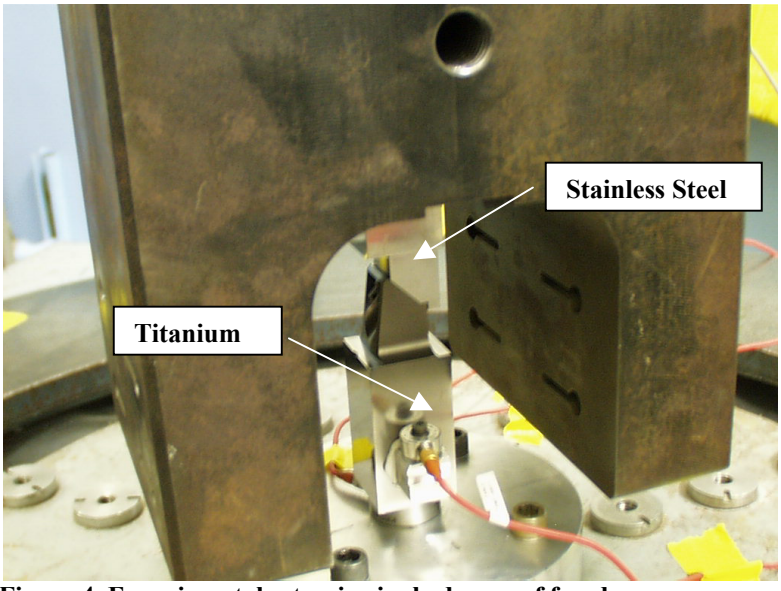

Figure 4. Experimental setup in single degree of freedom configuration.

The experiment can be represented as a base driven SDOF system as shown in Figure 5. The inertial mass is the mass, *m*, and the base is driven by the force, *f*. A linear spring, *k*, and a linear damping element, *c,* represent the linear part of the specimen. The nonlinear restoring force is lumped into *r*.

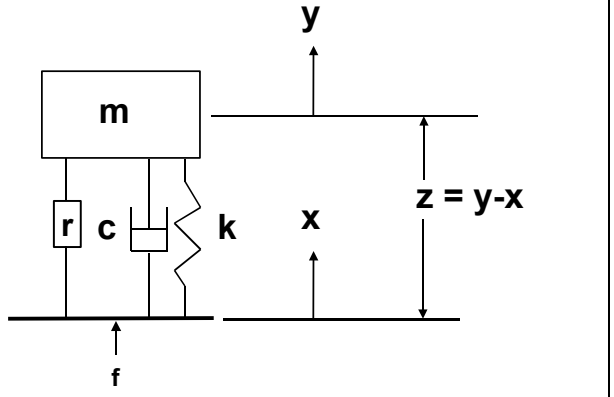

Figure 5. Model of experiment.

Measuring Energy Loss Per Cycle

The motion-to-motion transmissibility of a viscous damped base excited SDOF system is given by the well-known equation [6]

$$T = \sqrt{\frac{1+(2\zeta\omega/\omega_n)^2}{(1-\omega^2/\omega_n^2)^2+(2\zeta\omega/\omega_n)^2}} \tag{1}$$

where ω is the frequency and ζ is the viscous damping ratio.
At the undamped resonant frequency, ω_n, $\omega/\omega_n = 1$ and for $\zeta << 1$ the transmissibility is approximately

$$T \approx 1/2\zeta \tag{2}$$

For this discussion the motion measures of interest are the acceleration of the base and mass. For this system the force at the base is just the mass acceleration multiplied by the mass. Therefore the driving point accelerance (base acceleration / base force) is the reciprocal of the transmissibility divided by the mass.

The transmissibility at resonance is called the amplification factor or quality factor, Q, $(Q = T(\omega_n) = 1/2\zeta)$ of the system. The damping factor is related to the viscous damping coefficient by

$$c = 2m\zeta\omega_n \tag{3}$$

For this experimental system the quality factor is the mass acceleration divided by the base acceleration.
For forced harmonic motion at frequency, ω, and with displacement amplitude, Y, Thomson [8] defines an equivalent viscous damping, c_{eq}, for systems with other types of damping on the basis of an equivalent energy dissipated per cycle, E.

$$E = \pi c_{eq} \omega Y^2 \tag{4}$$

When the frequency of motion is $\omega = \omega_n$ this gives

$$E = \frac{\pi m A_m^2}{Q \omega_n^2} = \frac{\pi m Q A_b^2}{\omega_n^2} \tag{5}$$

Where
A_m = Acceleration of mass
A_b =Acceleration of base
$Q = A_m/A_b$=Quality Factor
$A_m >> A_b$ and $A_m = \omega_n^2 Y$

Experimental Results

Steady State Sine Vibration Experiments

Experiments were performed to measure the energy loss per cycle for a sinusoidal input force over a range of loads of 60, 120, 180, 240, and 320 lb-peak with the specified torque of 85 inch-lb resulting in a computed normal force of approximately 1700 lb.

The over-sized hole in the forward mount allows significant variation in alignment to occur unless efforts are made to minimize the effect. The oversized hole in the leg and the interaction of the interface and the bolt head with the hole is the suspected major source of variation in the response of the system from assembly-to-assembly of the same joint. A finite element analysis was performed using ABAQUS [7] to calculate the normal pressure in the interface due to the bolt preload. ABAQUS was used for convenience because the original quasi-static analyses were performed with this code. The results of the analysis are shown in Figure 6. The analysis shows the normal pressure is extremely high near the edge of the bolt hole and decreases rapidly away from the hole.

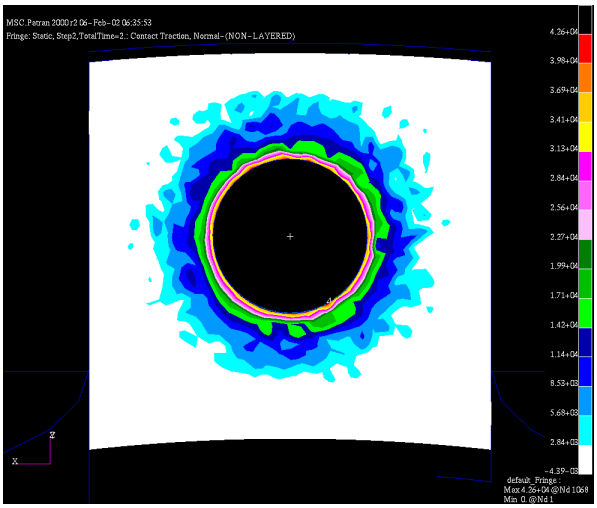

Figure 6. Normal pressure in interface due to bolt preload.

The energy loss per cycle was experimentally determined by performing a sine sweep controlling the force at a constant value over a frequency bandwidth encompassing the fixed base resonance of the test system. The fixed base resonant frequency of the system ranged form 269 to 278 Hz depending on the excitation level and varied slightly for each assembly of the bolted connection. The amplitude ratio (transmissibility) between the acceleration of the mass and the acceleration of the base was then calculated to determine the amplification factor (Q). A constant bandwidth (10Hz) digital tracking filter was used with a linear sweep rate of 0.50 Hz per second in the signal processing to compute Q. The amplification factor was established at the frequency where the phase was measured to be 90 degrees.

Single Leg Experiments With a Controlled Gap Opening

Data were collected for a total of nine load cycles. A load cycle encompassed cleaning the surfaces and reassembling the joint and then performing sweeps at each of the five force levels. For the first series of experiments a precision 0.010-inch shim was used to set the spacing in the joint each time to obtain as repeatable an experiment as possible.

The energy loss per cycle data versus force for the nine experiments are shown in Figure 7 in a log-log plot that indicates the straight-line character of the data. This straight-line relationship indicates that there is a power law relationship between the energy loss per cycle and the input force, $E=kF^n$. The data are also shown on a linear plot in Figure 8 that illustrates the strong dependence of the energy dissipation on input force.

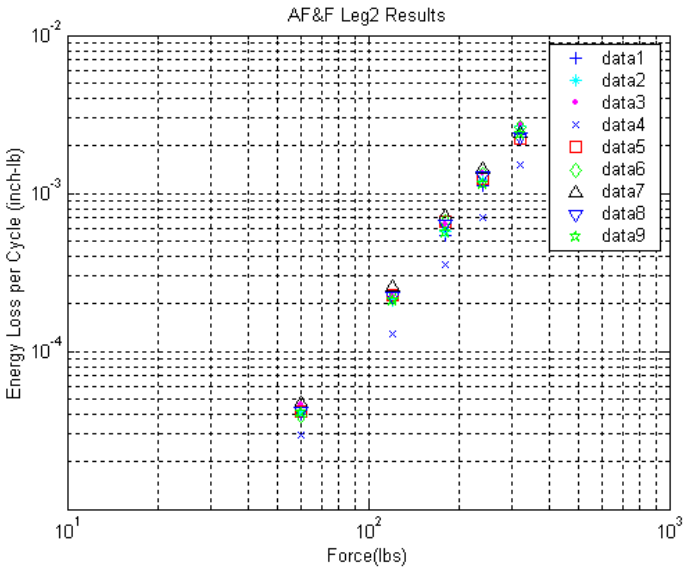

Figure 7. Log-log plots of force vs. energy dissipation curves.

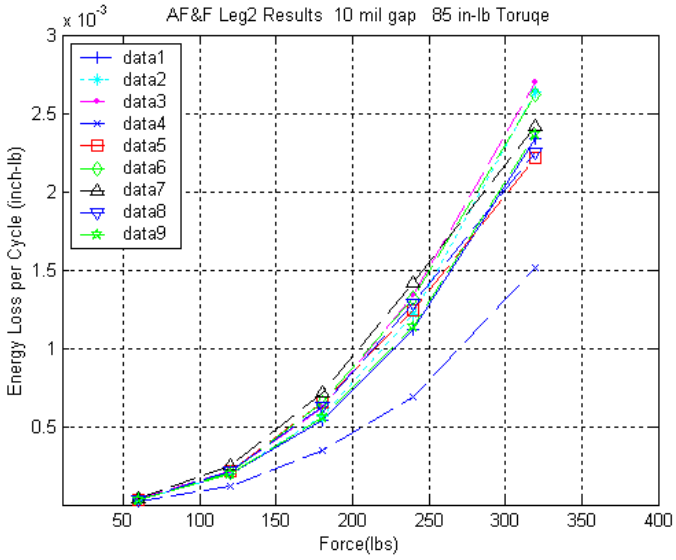

Figure 8. Linear plot of force vs. energy dissipation curves.

The data tend to fall relatively close to each other with the exception of experiment number four which shows much less dissipation than the other experiments. It appears that the system was "locked-up" for this trial, but for subsequent experiments returned to similar levels as previous experiments. The data show that even though one set of hardware was used in all experiments, variation due to repeated disassembly and assembly is on the order of 20 to 30 percent (excluding outlying data from experiment number four). The experimental results plotted with the mean and standard deviation are shown in Figure 9. The data, with the exception of experiment number four, fall within one standard deviation of the mean.

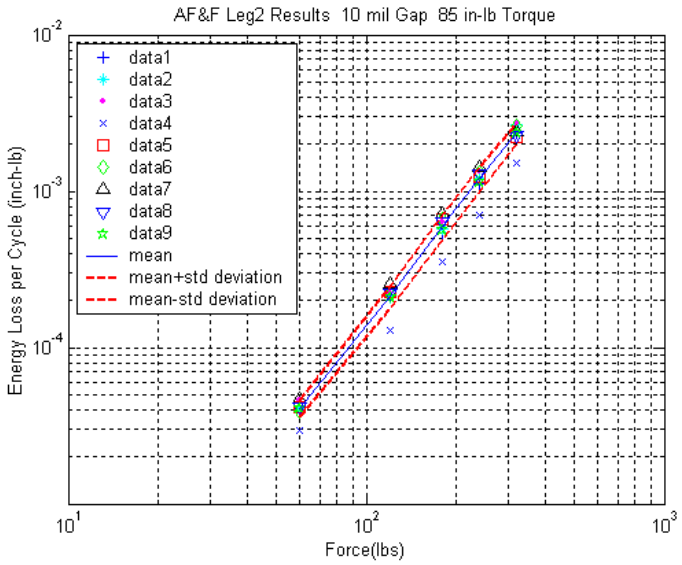

Figure 9. Energy dissipation curves with mean and standard deviation.

The slopes of the energy curves, shown in Figure 10, were found by fitting a straight line to each set of the log-log data and were found to be very repeatable with an average slope of 2.429 and a standard deviation of 0.05218. This indicates that although the overall amplitude of the energy loss may vary 20-30 percent, the slope of each energy curve seems to be very repeatable. This is an important observation because the slope of the energy dissipation curve is an important parameter in establishing reduced order models for joint models such as the Iwan model and Smallwood's 3-parameter model [1,2,3]. The slopes are also plotted as a function of the Test Run Number (Experiment Number) and shown in Figure 11. The results do not indicate any significant trend associated with wear of the surfaces over the first set of experiments.

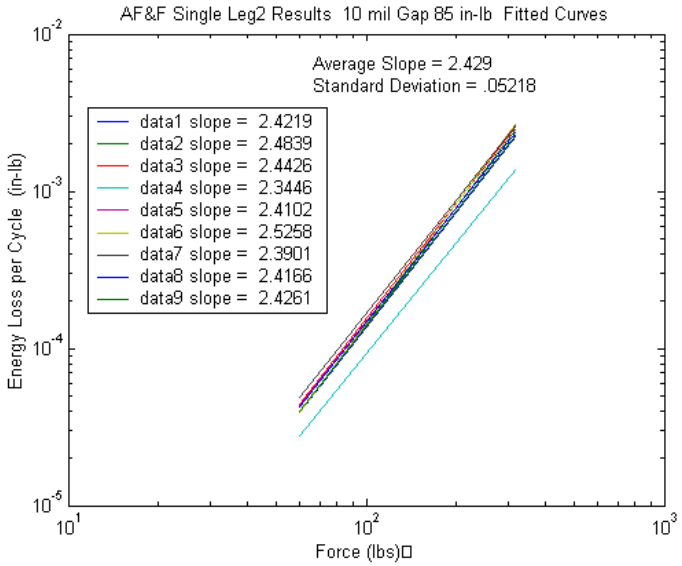

Figure 10. Straight line fit to energy dissipation data.

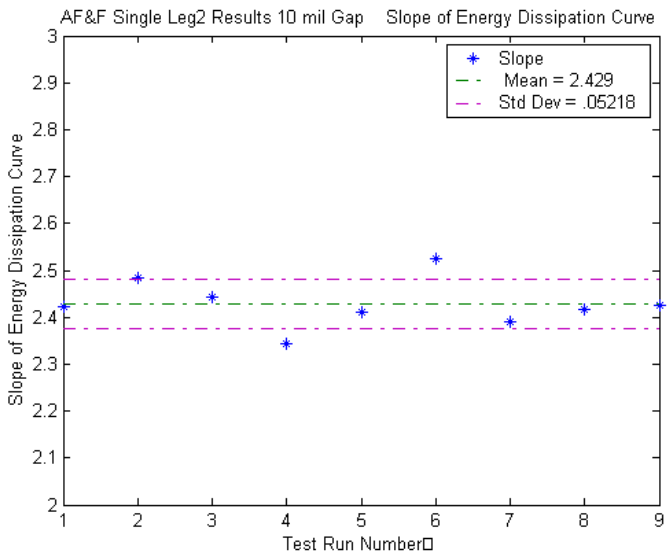

Figure 11. Slope of energy dissipation for each test run.

Single Leg Experiments With a Closed Gap

A total of seven load cycles were preformed with the vertical gap closed (light contact condition) to investigate the effect of the interaction of the additional interface. The results, shown in Figure 12 through Figure 14, indicate similar levels of dissipation as for experiments with the vertical gap open, but with slightly higher variation among the trials. The data were fit with straight lines, and the slopes computed along with the statistics and are listed in Figure 13. The mean slopes were very similar (2.429 and 2.410) between the 0.010 gap experiments and the experiments with the gap closed. The primary effects of the additional contact seem to be a slight increase in the energy dissipation and an increased variability due to the differences in assembly.

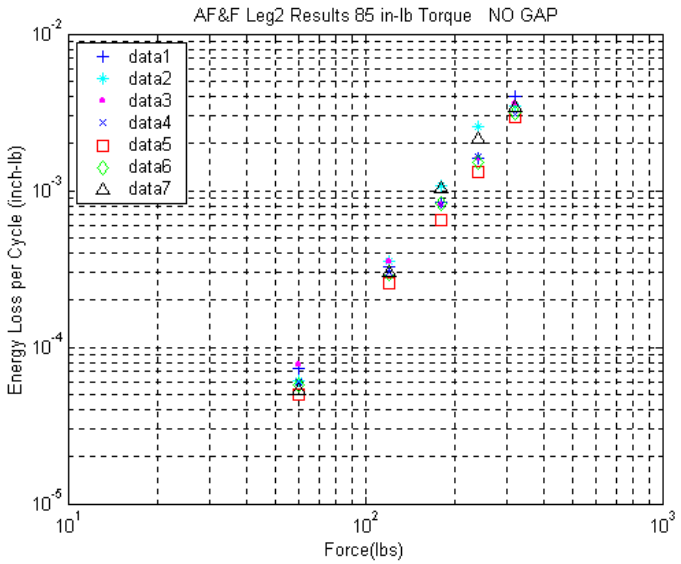

Figure 12. Energy dissipation curves with no gap in interface.

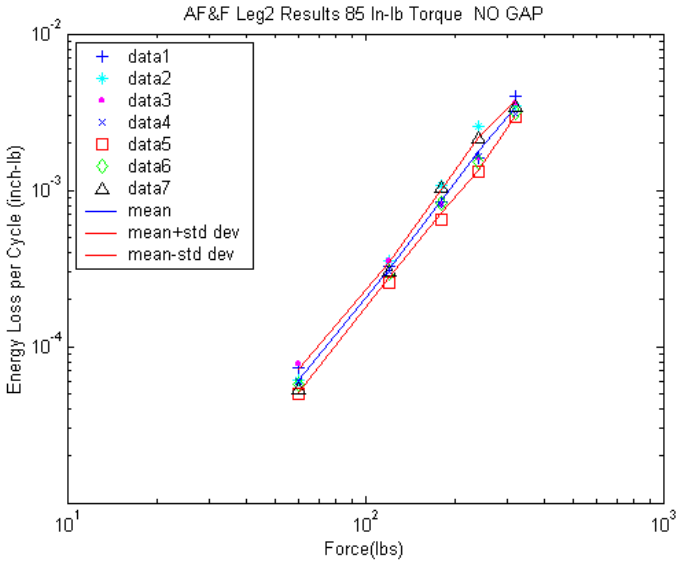

Figure 13. Energy Dissipation Curves with Mean and Std. Deviation.

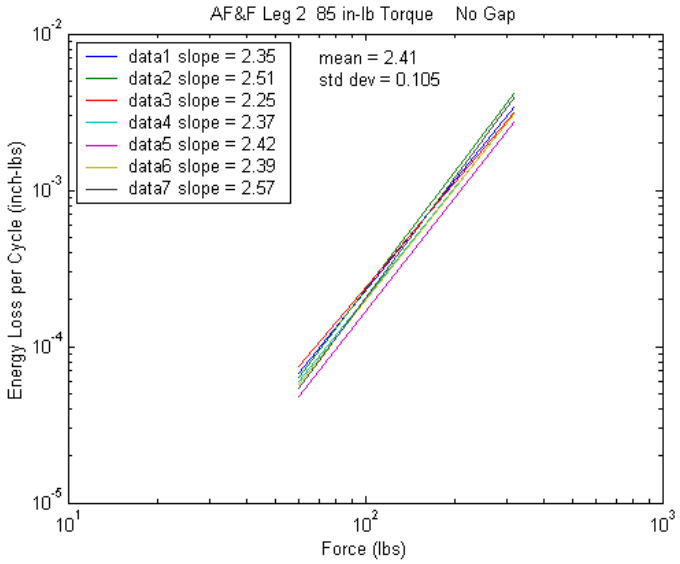

Figure 14. Straight line fit to energy dissipation curves with no gap.

Solid Single Leg Experiments

A similar set of experiments were performed for a geometrically identical solid-leg made of stainless steel with no frictional interface. The purpose of the experiments was to establish a lower limit for the unaccounted loss mechanisms in the experiment and to allow the contribution due to the joint to be identified. It is acknowledged that the solid-leg will not have the same stiffness as would a single piece composite (both titanium and stainless steel-- physically impossible to construct) solid-leg of titanium and stainless steel, but the

internal material damping of stainless steel and titanium are both very low and well below the damping introduced by a bolted interface.

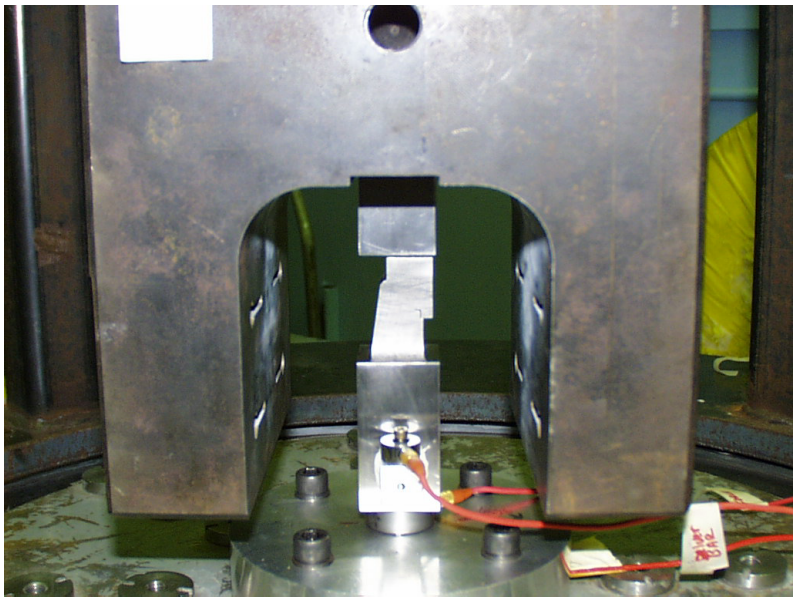

Figure 15. Solid leg experimental setup.

The results for the solid single leg are shown in Figure 16 for five load cycles. The measured natural frequencies for the solid leg experiment ranged from 362 to 364 Hz. These were considerably higher than the jointed single leg whose natural frequencies ranged from 273 to 278 Hz. These frequency differences illustrate the reduction in stiffness in a bolted joint vs. a solid geometry. The data for the solid single leg was very repeatable as might be expected from a linear structure without the uncertainty of a bolted connection.

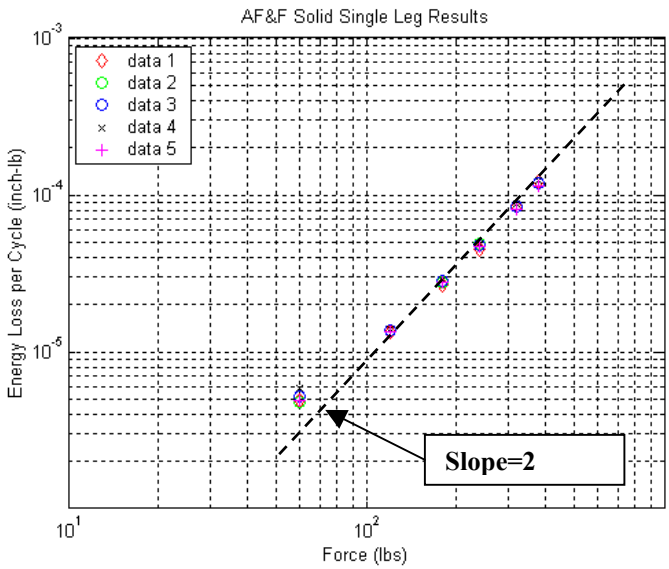

Figure 16. AF&F solid leg results.

The energy dissipation at the lower force levels were very small and difficult to measure experimentally. At the lower force levels the measurement of the amplification factor Q was limited by the noise floor of the measurement system. The data are shown plotted with a line with a slope of two in Figure 16. As can be seen at low force levels the data do not follow the theoretical slope of two for a linear system, however, at higher force levels with better signal-to-noise the data closely follow the theoretical slope.

The solid and jointed single leg data are plotted together in Figure 17. The data show the significant increase in energy dissipation introduced by the presence of the bolted connection. The data also show the difference in slopes of the energy curves between the two systems resulting in much increased energy dissipation for the jointed connection as the input force increases.

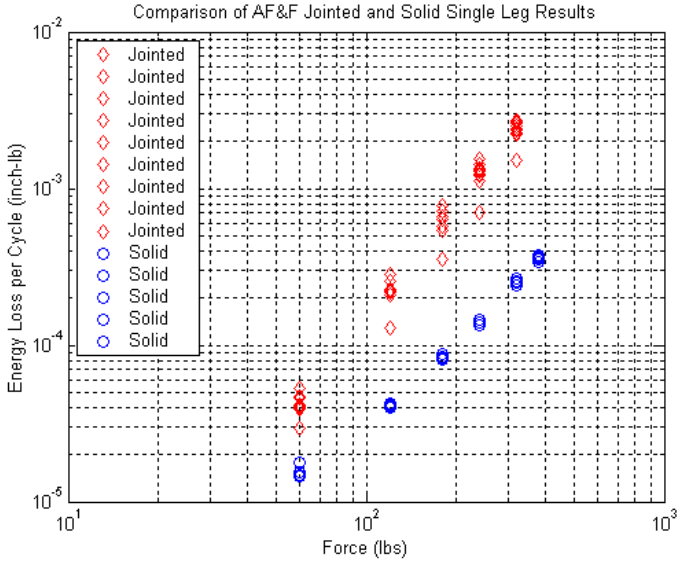

Figure 17. Comparison of solid and jointed single leg.

Load History Effects

The experiments demonstrated load history effects that were also noted for simple lap joint experiments [5]. The amplification factor, *Q*, would increase with the number of vibration cycles. When the bolted joint was disassembled and reassembled with the same torque the system would return to similar starting point with a lower amplification factor (higher damping) and then follow similar trend of decreasing damping. A total of seven experiments were performed with an input force of 120 pounds. For each experiment a total of four sinusoidal sweeps were performed and the equivalent viscous damping ratio $\zeta \approx \frac{1}{2Q}$ was computed and plotted as a function of the cumulative number of vibration cycles in Figure 18. As can be seen, the equivalent damping ratio decreases in an asymptotic fashion as the number of cycles of vibration increases. The mean of the data varies from approximately 0.4 to 0.3 percent of critical damping over approximately 28,000 cycles of vibration (approximately 2 minutes at 275 Hz). This is a change of approximately 25 percent in the damping ratio.

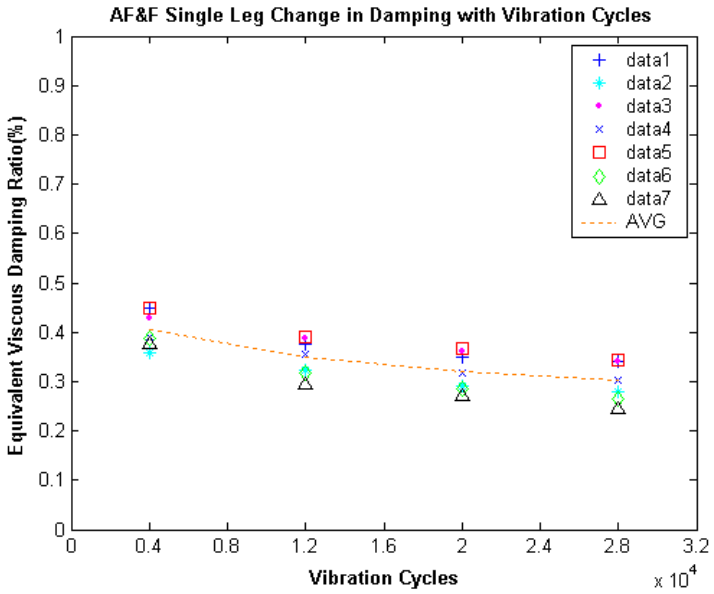

Figure 18. Load history dependence of single leg damping.

Base Hysteresis Measurements

The non-linear response of the single-leg experiment was further investigated by computing the hysteresis curves computed from the input force and the motion of the base. As discussed in Reference [5] the base hysteresis curve developed at resonance provides a sensitive measure of the non-linear response of the system.

The energy dissipated during steady state response in a single input passive system must be equal to the energy supplied at the input to the system to sustain the steady state response. For a simple harmonic input the input energy per Thomson [8] is

$$E = FX \sin\phi \tag{7}$$

Where F is the magnitude of the force input, X is the magnitude of the base displacement and ϕ is the phase angle between the force and displacement. The relationship between the magnitude of the acceleration and the magnitude of the displacement at the frequency, ω, is simply

$$A = -\omega^2 X \tag{8}$$

Only the component of displacement out of phase with the force will dissipate energy. At resonance, $\phi = 90$ degrees, and $\sin\phi = 1$. The orthogonality of sine and cosine functions shown in Equation 9 assures that if either the force or acceleration is a pure sinusoid, sin θ, then harmonic distortion, sin $n\theta$, in the other measure will not dissipate energy.

$$\int_0^{2\pi} \sin n\theta \sin m\theta d\theta = 0 \quad \text{For n} \neq \text{m} \tag{9}$$

$$\int_0^{2\pi} \cos n\theta \cos m\theta d\theta = 0 \quad \text{For n} \neq \text{m}$$

Only the fundamental component will dissipate energy. If both the force and displacement of the base are distorted then the harmonics can dissipate energy. At resonance almost all the harmonic distortion observed in the experiments was in the base acceleration waveform. The inertial mass acceleration waveform was nearly a scaled version of the base input force, $A_m=F/M$.

At the resonance, the inertia and stiffness forces balance. The motion required at the base to maintain a steady state response with a prescribed force is very small for a lightly damped system. In order to estimate the small base motion in the presence of background shaker and instrumentation noise, additional knowledge about the response of the system to sinusoidal excitation was leveraged. If a linear system is excited by a sinusoidal force at frequency, ω, the response will occur at exactly that same frequency. If the excited system is nonlinear, higher harmonics may be evoked, but the orthogonality discussed above assures that all of the energy will reside in the first harmonic. If the excitation is at a fundamental frequency and several of its harmonics, the dissipation consists of components associated with motions at the fundamental and all harmonics common to both the force and the motion.

This knowledge was applied by fitting a best least squares fit to the measured base acceleration with a sum of phase shifted sinusoids at the fundamental frequency and higher harmonics. In other words, the Fourier coefficients of the base motion were calculated. This signal processing selectively filters the response at only the fundamental frequency and its harmonics, discarding all other portions of the measured signal due to noise (assuming that power line frequency and harmonics do not coincide with the resonant frequency and harmonics i.e. 60 Hz, 120 Hz, 180 Hz, etc.). It was determined by fitting the data with varying numbers of harmonics that maintaining fundamental and five harmonics was sufficient to represent the periodic component of the base motion. Very little was gained by including yet higher harmonics.

The Fourier coefficients indicate that the second harmonic is very strong in the base motion and that is an indication of asymmetric motion between tension and compression of the joint. Asymmetric waveforms tend to require the addition of even harmonics for their Fourier series representation as compared to symmetric waveforms that may require only odd harmonics. A typical set of Fourier coefficients for the base acceleration is shown in Table 1. Note that the amplitude of the second harmonic (twice the frequency of the fundamental) is higher than the fundamental amplitude. The asymmetry between tension and compression arises from at least two effects, first the difference in the joint stiffness between tension and compression and second, the normal traction is significantly higher on the compression part of the cycle thereby increasing the resisting frictional force in the

interface. The corresponding Fourier coefficients for the input force and acceleration of the mass are given in Table 2 and Table 3.

Table 1. Fourier coefficients of typical base acceleration for 60lb force input.

Harmonic #	Frequency (Hz)	Acceleration Amplitude (g)	Phase (Radians)
1 (Fundamental)	2.79E+02	1.60E-03	-9.23E-01
2	5.57E+02	3.08E-03	-2.49E+00
3	8.36E+02	4.74E-04	3.84E-01
4	1.11E+03	4.74E-04	-2.86E+00
5	1.39E+03	1.73E-04	-2.84E+00
6	1.67E+03	3.17E-04	-2.37E-01

Table 2. Fourier coefficients of typical 60lb force input.

Harmonic #	Frequency (Hz)	Force Amplitude (lbs)	Phase (Radians)
1 (Fundamental)	2.79E+02	6.02E+01	6.43E-01
2	5.57E+02	7.13E-01	2.98E+00
3	8.36E+02	2.11E-02	-2.15E+00
4	1.11E+03	5.08E-03	3.88E-01
5	1.39E+03	2.85E-03	3.45E-01
6	1.67E+03	1.81E-03	9.95E-02

Table 3. Fourier coefficients of typical mass acceleration for 60lb force input.

Harmonic #	Frequency (Hz)	Acceleration Amplitude (g)	Phase (Radians)
1 (Fundamental)	2.79E+02	3.21E-01	-2.50E+00
2	5.57E+02	3.81E-03	-1.64E-01
3	8.36E+02	1.00E-04	6.72E-01
4	1.11E+03	2.51E-05	2.37E+00
5	1.39E+03	2.85E-05	-1.77E+00
6	1.67E+03	3.10E-05	-2.78E+00

The reconstructed time histories using the Fourier coefficients were calculated by summing the harmonic components

$$a(t) = \sum_{k=1}^{N} A_k \sin(2\pi k f_0 t + \phi_k) \tag{10}$$

Where:

A_k =Amplitude of kth component
f_0 = Fundamental frequency
ϕ_k= Phase of kth component

The reconstructed time histories for the force, mass acceleration, and the base acceleration are shown in Figure 19 through Figure 21. As can be seen the harmonic distortion of the force and mass acceleration are minimal while the harmonics in the very small base acceleration are very pronounced. The nonlinear behavior of the joint experiencing microslip is revealed much more in the small base acceleration than in the mass acceleration or force where the linear portion of the response dominates the small non-linear component. The harmonic distortion in the displacement decreases rapidly with increasing frequency because for a given acceleration the corresponding displacement decreases as a function of the frequency squared.

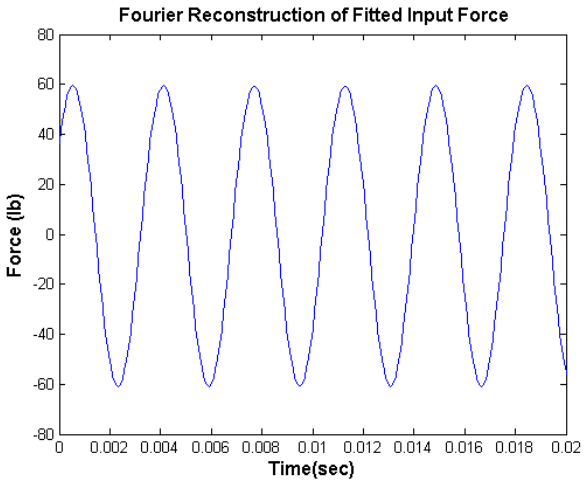

Figure 19. Reconstructed input force.

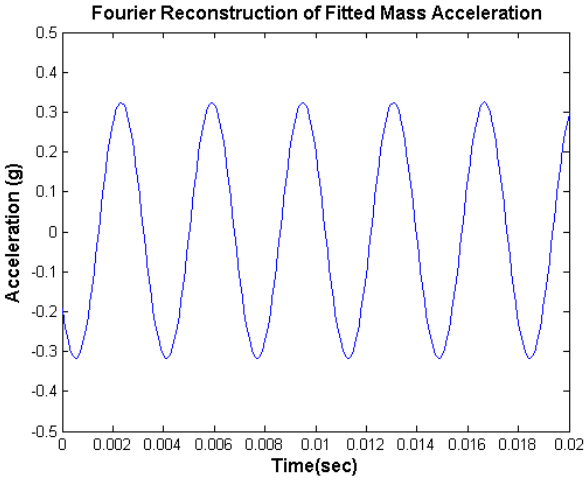

Figure 20. Reconstructed mass acceleration.

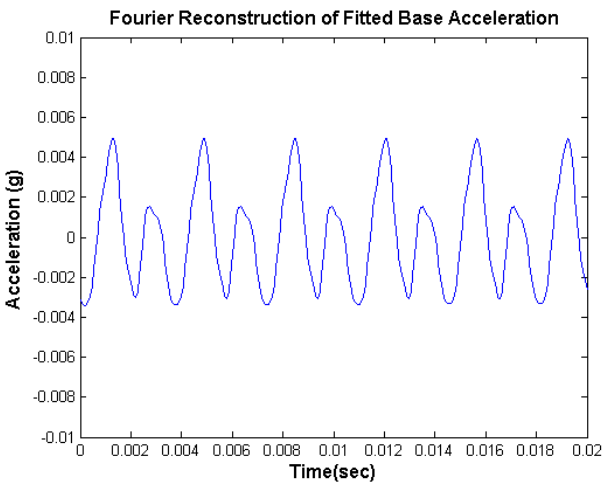

Figure 21. Reconstructed base acceleration.

Utilizing the analytical fit to the measured signals, the force versus base motion hysteresis curves were computed for both the solid leg and the jointed leg for selected experiments. Since the linear portion of the response to a harmonic input is contained in the response at the fundamental frequency, the force vs. linear portion of the base displacement should plot as an ellipse for a linear system. Deviations from the ellipse are a measure of the nonlinear response. Typical force versus base motion hysteresis curves are shown for 60 and 320 pounds of force in Figures 22 and 23. The solid leg hysteresis curves are much more elliptical than are the hysteresis curves for the jointed leg. The area within each curve is a measure of the energy dissipated per cycle. Note the significant difference in area for the jointed leg compared to the solid leg. The asymmetry of the response between compression and tension is also very evident in the plot. The loop shown in the jointed leg is due to the large second harmonic component that increases with increasing force level.

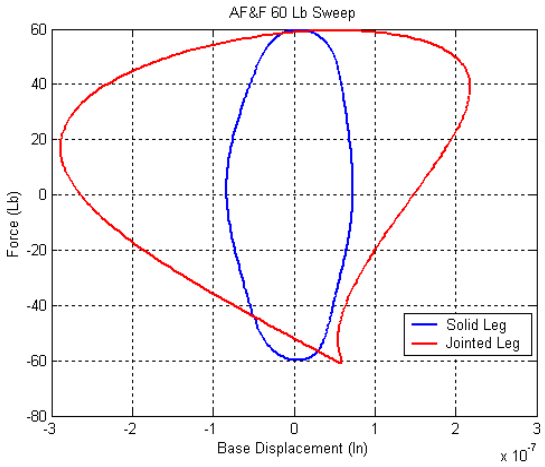

Figure 22. Force vs. base motion hysteresis curves for a 60 lb sweep.

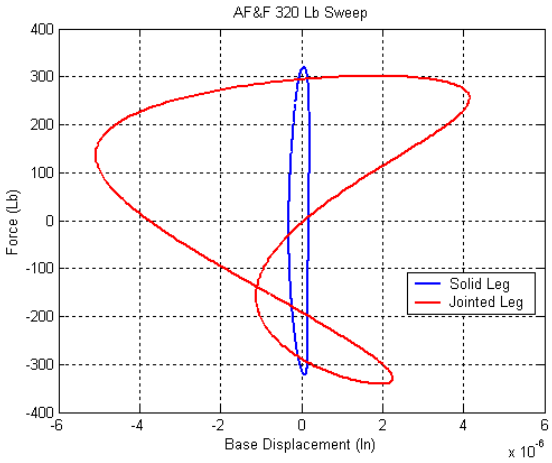

Figure 23. Force vs. base motion hysteresis curves for a 320 lb sweep.

The energy loss per cycle was computed three ways for selected load cycles. The first technique utilizes Equation 5 with measured Q at resonance. The second uses the derived Fourier coefficients for the mass acceleration and base acceleration to compute the relative displacement and integrates the force vs. relative displacement hysteresis curve. The third technique uses the derived Fourier coefficients of the base acceleration to integrate the area under the force vs. base displacement hysteresis curves. A typical comparison of the computed energy loss per cycle from these techniques is shown in Table 4. The calculations using Q at resonance yields numbers that are within approximately 12 percent or less of those computed by the methods that involve fitting the force and acceleration signals and computing the hysteresis curves. This is encouraging in view of the very small magnitude of the numbers associated with the base motion of a few micro-inches or less.

Table 4. Comparison of energy loss per cycle calculations.

Input Force (lb)	Resonance (in-lb)	Force vs. Relative Displacement (in-lb)	Force vs. Base Displacement (in-lb)
60	3.805E-05	3.683E-05	3.768E-05
120	1.956E-04	1.893E-04	1.893E-04
180	5.207E-04	4.907E-04	4.905E-04
240	1.066E-03	9.759E-04	9.755E-04
320	2.242E-03	1.958E-03	1.957E-03

Random Vibration Experiments

Experiments were performed to investigate the response of the single-leg system to random vibrations. A constant force power spectral density at two levels was controlled over a bandwidth encompassing the fixed base resonance of the system. The spectral density was adjusted to achieve peaks in the time history of the force consistent with the peaks used for the sinusoidal excitation to allow comparison with the two types of excitation. The first level was performed at 20 lb-rms in order to yield three-sigma peaks in the Gaussian random vibration signal of 60 lb. The second level was performed at 107 lb-rms in order to

yield peaks of 321 lb. Frequency response functions (FRF) were computed from the acceleration of the inertial mass, y, with respect to the base acceleration, x, using the ratio of the cross-spectral density to the auto-spectral density,

$$H(f) = \frac{G_{xy}(f)}{G_{xx}(f)} \tag{11}$$

Where G_{xy} is the cross-spectral density between the base acceleration and the acceleration of the mass and G_{xx} is the auto-spectral density of the base acceleration.

The tests were controlled with maximum available 3200 frequency lines yielding a frequency resolution of 0.125 Hz. This very fine frequency resolution was required to resolve the peak (Q) in the measured FRF for the lightly damped system. The results are shown in Figure 24 including the magnitude of the FRF and the associated coherence functions for the two levels. For the 20 lb-rms input level the FRF looks smooth with a peak value near that computed with the sinusoidal input and the coherence function shows only a slight notch at the resonant frequency. At the higher 107 lb-rms input level the FRF shows the expected decrease in the peak value (Q) but also shows considerable distortion and noise near the peak. The coherence function is also noisy with a very sharp notch in the vicinity of the resonance. These effects are indications of non-linear response of the system that becomes more pronounced with increased input force level.

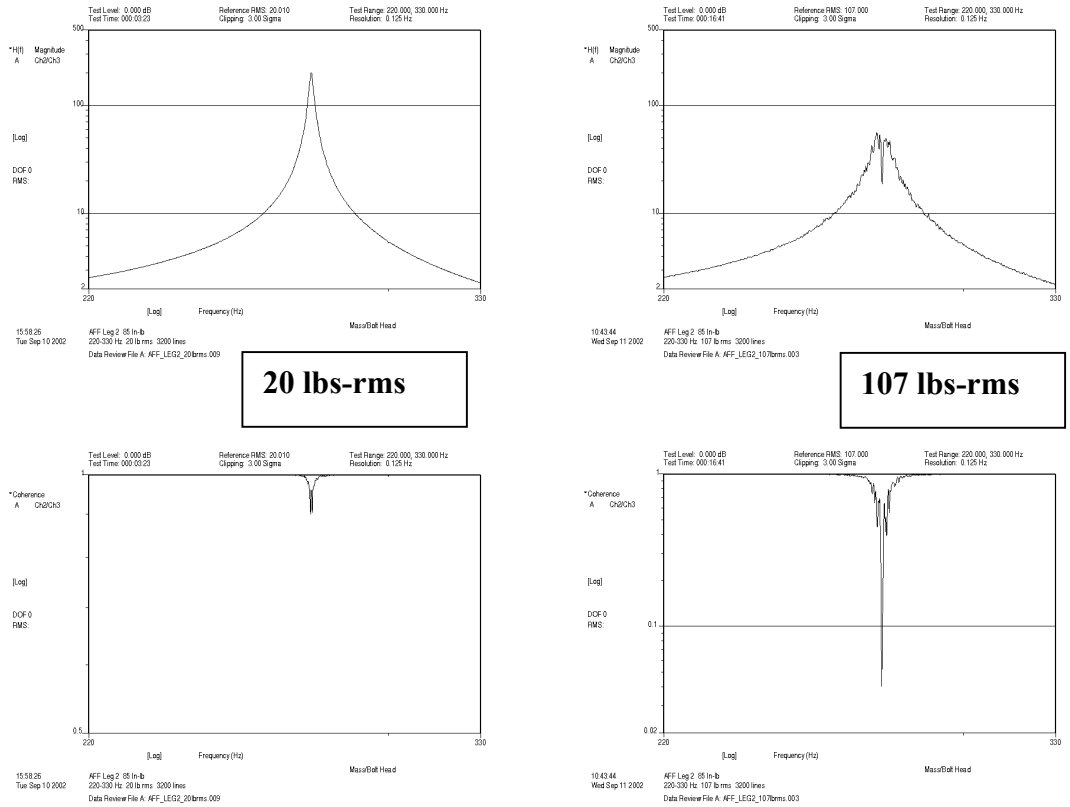

Figure 24. Frequency response function and coherence function measurements for random vibration at 20 lbs-rms and 107 lbs-rms.

Analytical Investigation of the FRF for a Non-linear System

To further investigate the sharp decrease in coherence and the noise on the calculated FRF an analytical study was performed with an idealized non-linear single degree freedom system. The equations of motion for a SDOF system with viscous damping and a cubic stiffness were used to calculate the transfer function and coherence of the system. The results were compared to the response of a linear SDOF system.

The following results were obtained with a simple model of a SDOF mass with spring and viscous damper. The spring in the model can be defined as linear, linear plus cubic, or bilinear. The natural frequency of the system is 300 Hz with the linear spring. The damping ratio is 0.2. A typical linear plus softening cubic spring appears has the restoring force shown in Figure 25.

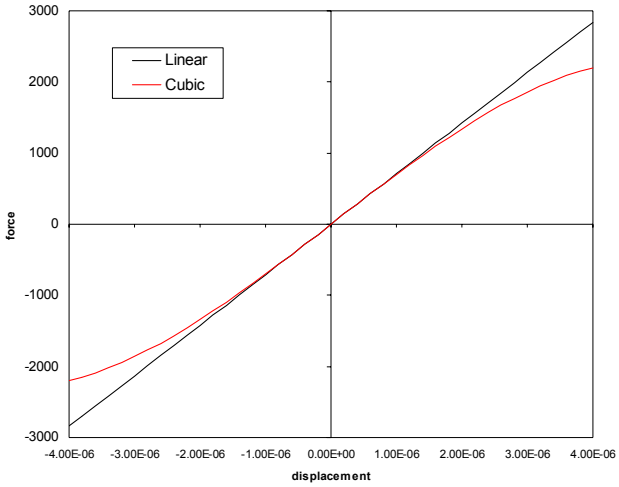

Figure 25. Linear and linear+cubic stiffness plot.

When both the linear and nonlinear SDOF systems were excited using band limited stationary random excitation whose autospectral density is flat over 100-500 Hz, the FRF's shown in Figure 26 were found. Note the distortion of the peak and the drop in coherence with the cubic stiffness component in the spring.

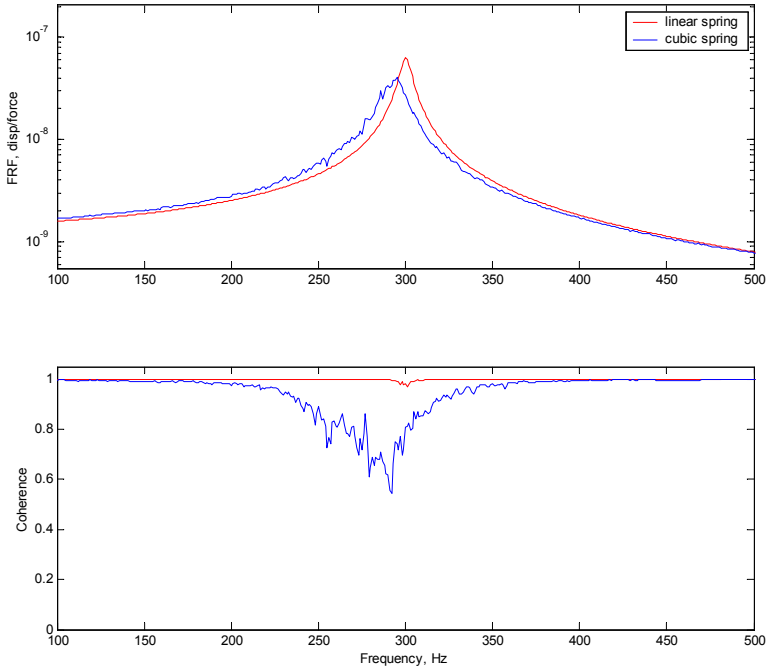

Figure 26. Analytical results for SDOF system with linear and cubic stiffness.

The analytical study shows that the FRF computed for an ideal non-linear system (with no noise) shows similar results as those observed in the experiments for the single leg

experiment. The single leg demonstrates both non-linear stiffness and non-linear microslip damping.

Transient Excitation Experiments

A separate experiment was performed to provide measured response of the single leg to a transient excitation. This measured response would then serve as a reference data set for comparison with a model prediction where the model parameters would be computed from the experimental sinusoidal data. The experimental system was bolted to a very large 32,000-pound block of steel to simulate a fixed base condition. The experimental setup is shown in Figure 27 and Figure 28. In order to bolt the base plate to the mass a new set of holes was required in the base plate. During this process the holes were drilled in the wrong location and an additional set of holes were then required. The effect of this was to decrease the stiffness of the base plate as compared with the stiffness when on the shaker with a single set of holes. Large one-inch diameter by approximately 0.5 inch thick hex nuts were used as spacers at four locations between the base plate and the surface of the large mass. These spacers were used to provide clearance for the accelerometer beneath the force gage and to simulate a similar contact condition provided on the shaker with the inserts in the armature. This shifted the frequency from approximately 270 Hz to 220 Hz for the jointed single leg test specimen and from 363 Hz to 260 Hz for the solid single leg.

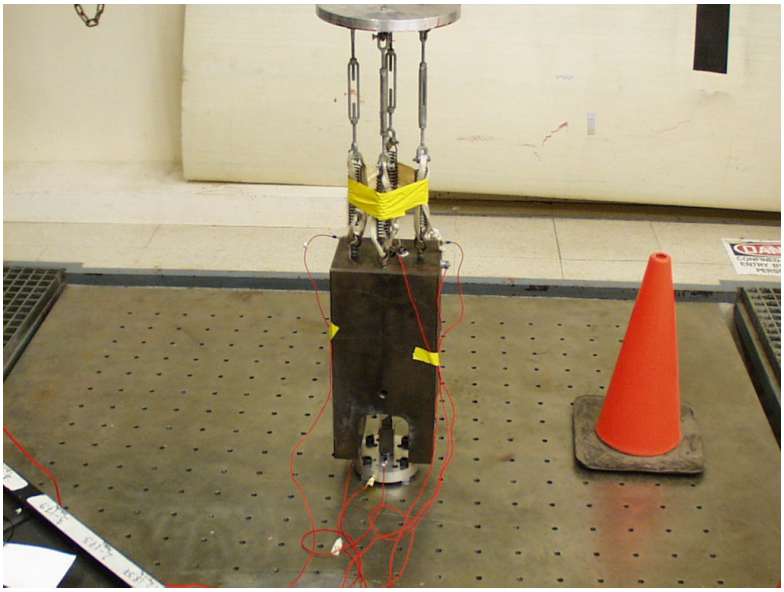

Figure 27. Experimental setup on seismic mass – View 1.

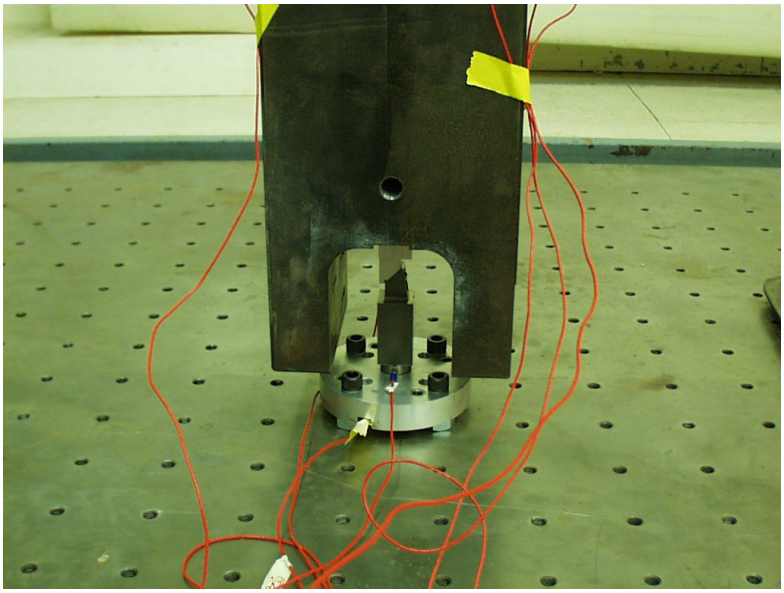

Figure 28. Experimental setup on seismic mass – View 2.

The top of the mass was impacted with an instrumented hammer and the response was measured with accelerometers and a force gage in the same locations as used for the sinusoidal excitation. The impact had to be applied slightly off-center since the large mass has a hole bored through its length at the center. This off-centered load did slightly excite the lower frequency bending modes of the system. Figure 29 is a plot of the transfer function between the accelerometer on the top of the mass and the input force. The major peak at about 220 Hz is the axial mode of the system. The other major peak at about 77 Hz is a bending mode of the system. In this figure it is evident that as the hammer force is increased, the quality of the response in the axial mode decreases and the response of the bending mode increases.

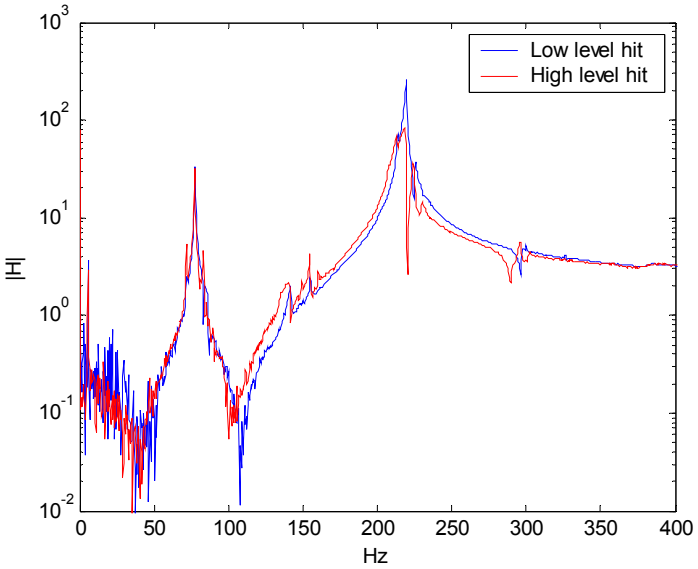

Figure 29. Frequency response function of acceleration response at top of the mass to hammer force input.

The impact level was adjusted to generate measured internal forces on the same order as were used in the sinusoidal excitation ranging from approximately 60 to 360 lb. The duration of the impact from the hammer was approximately one millisecond as shown in Figure 30. The small oscillation observed after the primary pulse is due to a small amount of ringing of the anti-aliasing filter.

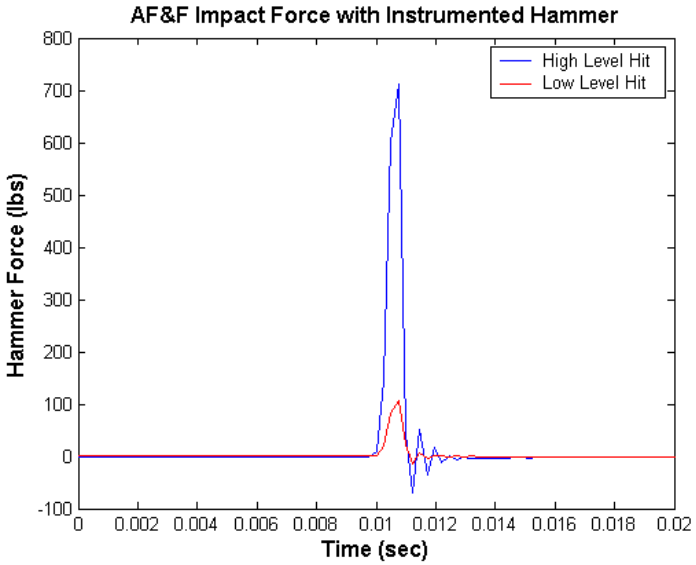

Figure 30. Hammer impact force.

The measured acceleration of the mass for the transient response is shown in Figure 31 and Figure 32. The slight modulation in the free decay is due to the participation of the bending modes at approximately 77 Hz. The participation of the bending mode in the response of the system is more prevalent with the high level impact indicating a non-linear coupling of the bending response with the axial response.

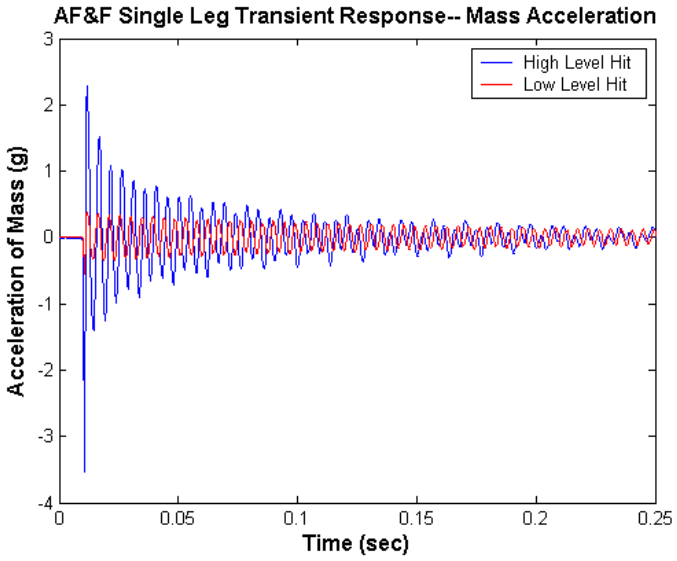

Figure 31. Mass acceleration time histories

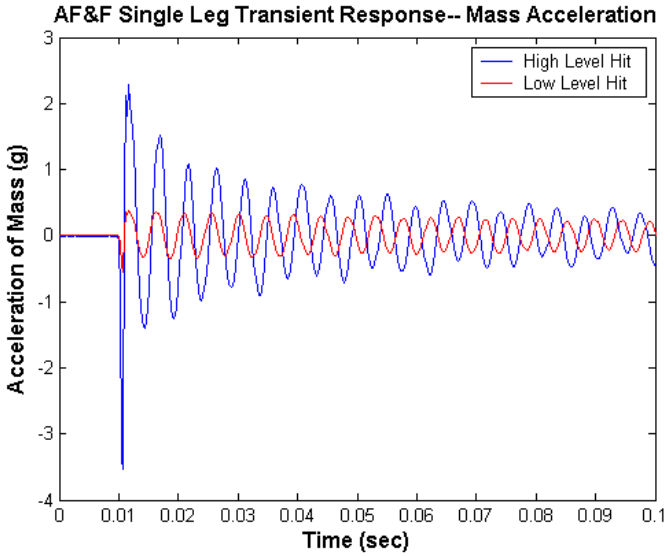

Figure 32. Expanded mass acceleration time histories

The bending mode response is much less obvious in the internal force measurement due to the fact that when bending is applied to the force gage the symmetry of gage will null the component due to bending. In Figure 33, the contribution of the bending mode at 77 Hz is much less than in the FRF for the acceleration response shown in Figure 29. When bending is applied to the force gage, half of the gage is subjected to increased compression, and the other half observes a decrease in compression. Since the polarity of the output is opposite they will tend to cancel.

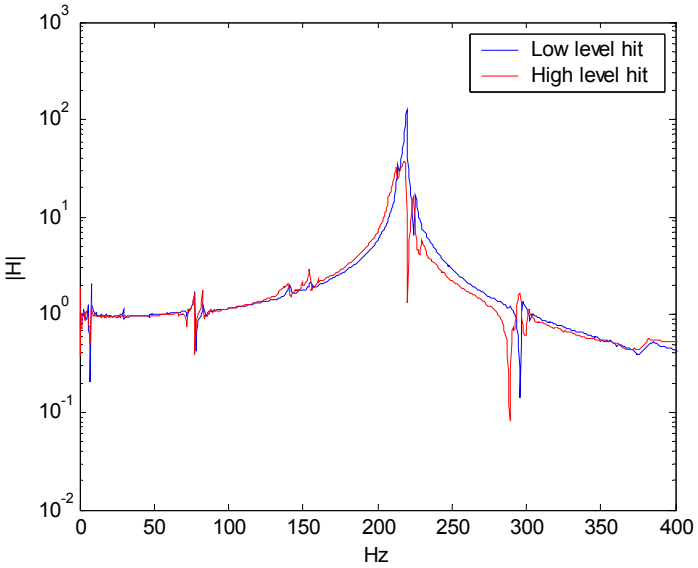

Figure 33. Frequency response function of the internal force response in the joint to hammer force input.

A plot of the internal force for the jointed structure for the high level and low level impacts is shown in Figure 34, and an expanded view of the early portion of the response is shown in Figure 35. The response of the system to the high level impact clearly shows the anticipated increased damping as evidenced by the increased relative attenuation of the amplitudes between successive peaks over the low level impact. The data also show the slight decrease in frequency with increasing amplitude due to the softening effect of the bolted connection.

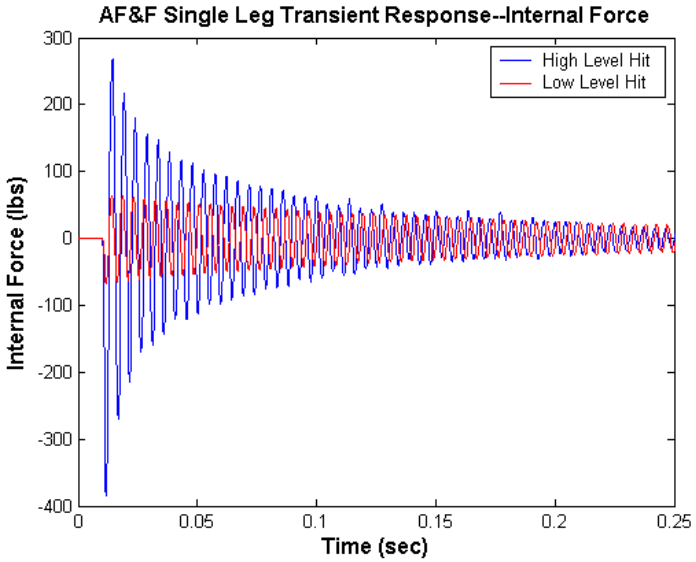

Figure 34. Internal force measurement.

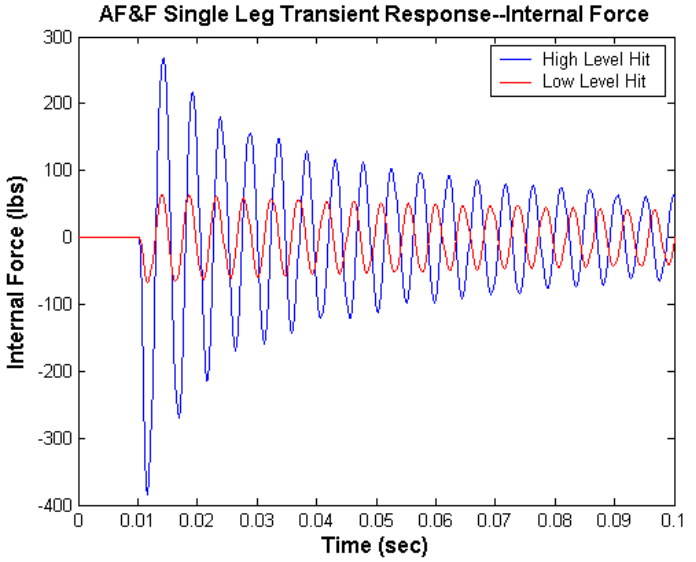

Figure 35. Expanded internal force measurement.

Since the internal force is directly related to the acceleration of the mass, the internal force signal, with less contamination due to the bending modes, was used for further calculations including the energy dissipation per cycle and equivalent viscous damping. The internal

force is also easily computed from the models and can be used for comparison with the model results.

The jointed single leg specimen was then replaced with the solid single leg, and the set of experiments was repeated to provide a reference set of results without the presence of the bolted joint. The responses for the measured internal force are shown in Figure 36 and Figure 37. As anticipated the damping of the solid single leg is much less than the jointed single leg as evidenced by the long duration required for the system transient response to decay (two seconds).

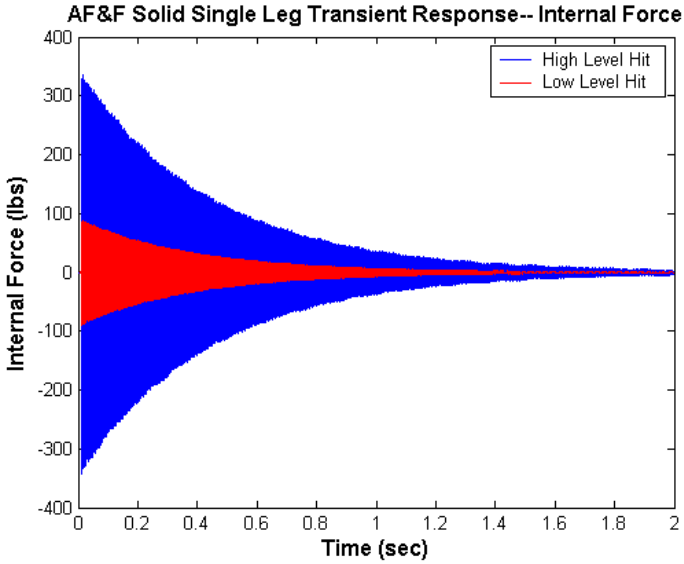

Figure 36. Internal force measurement for solid single leg.

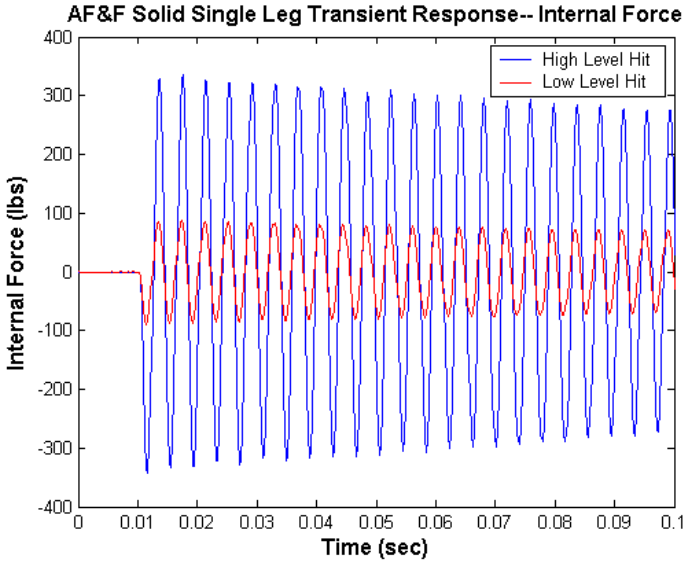

Figure 37. Expanded internal force for solid single leg.

The solid and bolted AF&F single leg results are compared in Figure 38 through Figure 41. The hammer impacts were not exactly the same for the jointed and solid tests but the significant differences in the response due to the bolted connection are apparent. The data show dependence of damping on amplitude because the rate of change of the response for the jointed specimen is much greater at the higher amplitude peaks, while the rate of change for the solid leg follows the classical exponential curve exhibited by linearly damped systems. It can also be seen that the damping for the jointed leg compares more closely to the damping for the solid leg for the low level hit, thus further illustrating the amplitude dependence of the damping due to microslip in bolted connections.

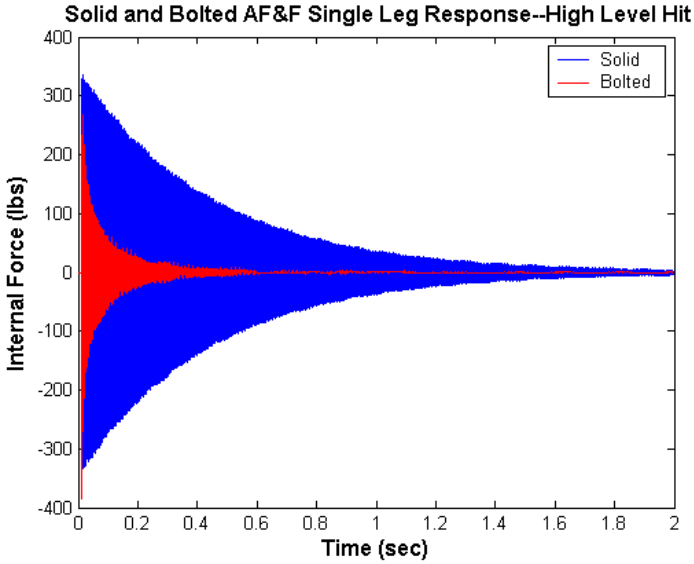

Figure 38. Comparison of solid vs. bolted for high level hit.

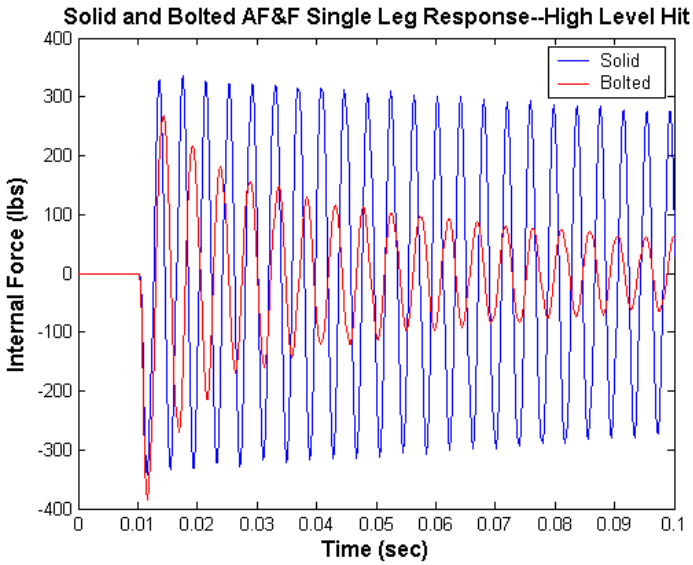

Figure 39. Comparison of solid vs. bolted for high level hit.

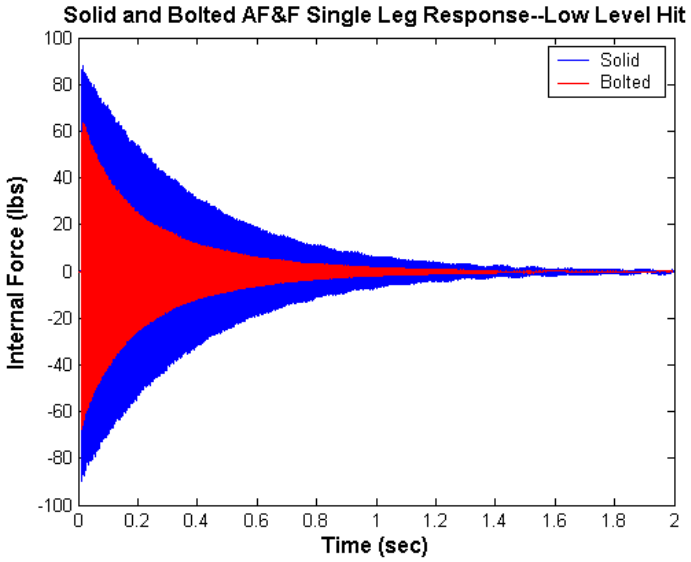

Figure 40. Solid vs. bolted for low level hit.

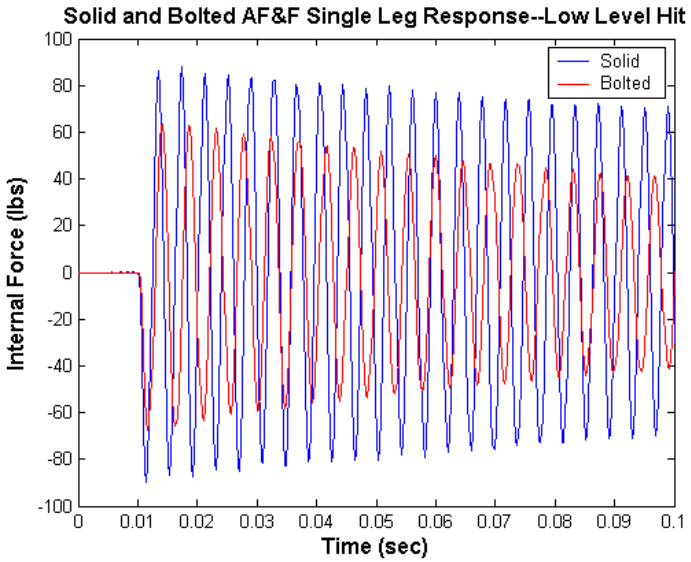

Figure 41. Expanded solid vs. bolted for low level hit.

Analysis of Transient Data

The decay of the transient responses can also be analyzed in order to derive a curve that describes the energy dissipation dependence on force amplitude. An advantage of this technique is that for a single impact with the hammer, the joint is exposed to a wide range of force amplitudes during ring down. The rate of decay of the transient response is related to the damping in the structure, and the damping is related to the energy dissipation.

Consider the free decay of a single degree of freedom system,

$$x(t) = e^{-\varsigma(t)\omega_n t}\cos(\omega_d t) \tag{12}$$

The envelope of the peaks is

$$x(t) = e^{-\varsigma(t)\omega_n t} \tag{13}$$

Taking the logarithm of both sides

$$\log(x) = -\varsigma(t)\omega_n t \tag{14}$$

and then, taking the derivative with respect to *t*, results in

$$\frac{d(\log(x))}{dt} = -\varsigma(t)\omega_n - \frac{d\varsigma(t)}{dt}\omega_n t \tag{15}$$

If the second term on the right side of Equation 15 is small with respect to the first term on the right, we can neglect it. In that case, the equivalent viscous damping, $\varsigma(t)$, is the slope of the envelope (log(*x*) as function of *t*) divided by the frequency.

For a linear system, the envelope of log(*x*) is linear. For jointed structures such as the bolted joint, a polynomial can approximate the points that define the envelope. The order of the polynomial that produces the best fit depends on the shape of the envelope. If the decay is relatively linear, a 3rd order fit is very good. If the decay is highly nonlinear (n>2.1 or so where n is the slope of the energy curve on a log-log plot) then a higher order fit works well. However, if the decay envelope is modulated by the presence of other modes in the response, then a higher order fit will attempt to match each ripple in the envelope and will yield an inaccurate estimate of damping. When n is about 2.2-2.4 and the response is fairly uncontaminated by other modes, a 5th or 7th order fit works well. Figure 42 shows the fit of a fifth order polynomial to the logarithm of peak amplitudes for a medium level hit. Figure 43 shows the same polynomial fit and peaks superimposed with the positive amplitudes of the transient response. As can be seen, the fit to the peaks is quite good.

The instantaneous value of the equivalent viscous damping ratio, $\varsigma(t)$, is obtained by computing the slope of the polynomial fit to the logarithm of the peak amplitudes and dividing by the natural frequency, ω_n, per Equation 15. These results are given in Figure 44 indicating the decrease in damping with time as the amplitudes diminish during the transient response.

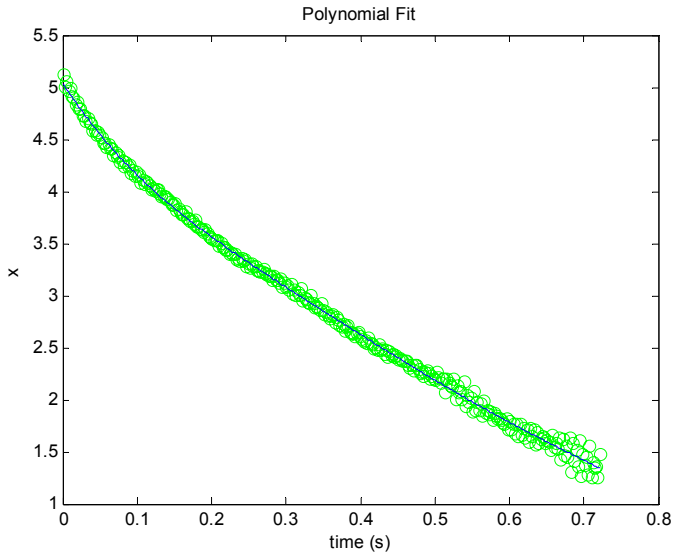

Figure 42. 5th order polynomial fit to the log of peak amplitudes for Medium Level Impact

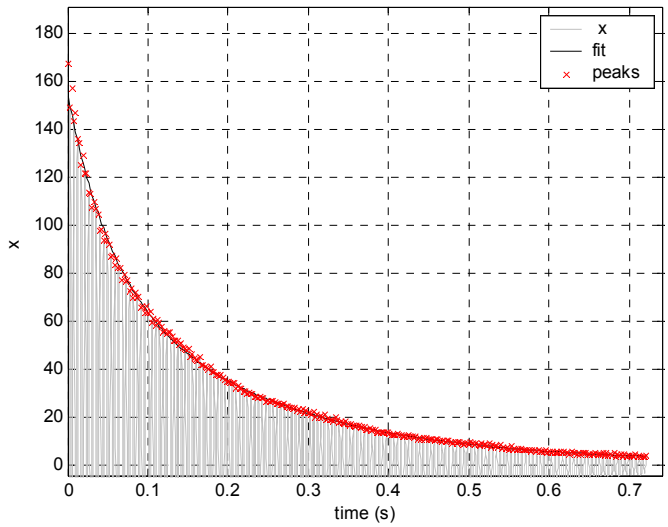

Figure 43. Polynomial fit and actual response.

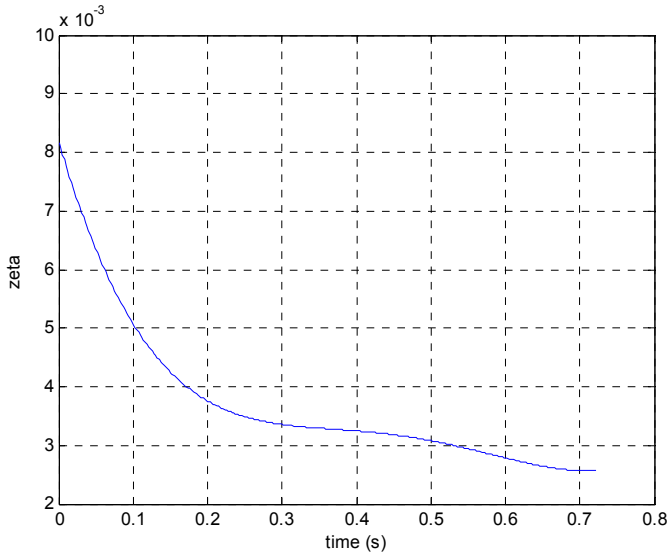

Figure 44. Zeta plotted as a function of time. Zeta is proportional to the slope of the fit seen in Figure 42.

Since the original response time history seen in Figure 43 is the force in the bolted joint versus time, the energy dissipation can be calculated based on the damping that was found for the decay. To convert equivalent viscous damping, $\varsigma(t)$, into energy loss per cycle, $E(t)$, use the formula

$$E(t) = \frac{k_m A_m^2}{Q f_n^2} = \frac{k_m m^2 A_m^2}{Q m^2 f_n^2} = \frac{2\zeta(t) k_m F^2(t)}{m^2 f_n^2} \tag{16}$$

Where,

$$Q = \frac{1}{2\zeta}$$

$$F = mA_m$$

$$k_m = 2\pi m$$

The constant k_m is multiplied by conversion factors in order to yield energy dissipation in units of in-lbs. A value of k_m = 6150 is used for our single leg experiments (which includes a mass of m~196 lbs). An example energy dissipated versus force curve is shown in Figure 45.

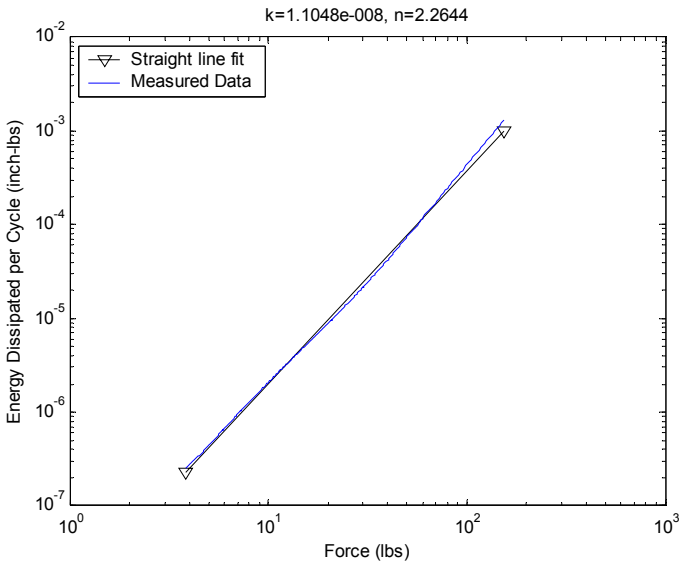

Figure 45. An example energy dissipation curve and its best straight line fit.

After the energy curve has been generated, a straight line fit can be calculated for the points of the curve in order to estimate the gain and slope of the curve in log-log space. These parameters can be used for various model predictions.

Transient Results

Four general levels of hammer forces were applied to the system in order to get energy dissipation data that encompass a wide range of internal forces and to see if there is any dependence of damping on initial force level. The lowest peak hammer force was about 80 lbs, and the highest was about 710 lbs. Five responses were collected for each of the four levels, adding up to 20 total responses. Derived energy dissipated per cycle versus force curves for all 20 responses of the jointed structure are seen in Figure 46. These curves contain values of energy dissipation and force for each peak in the transient response providing much high density of values than obtained from the sinusoidal experiments.

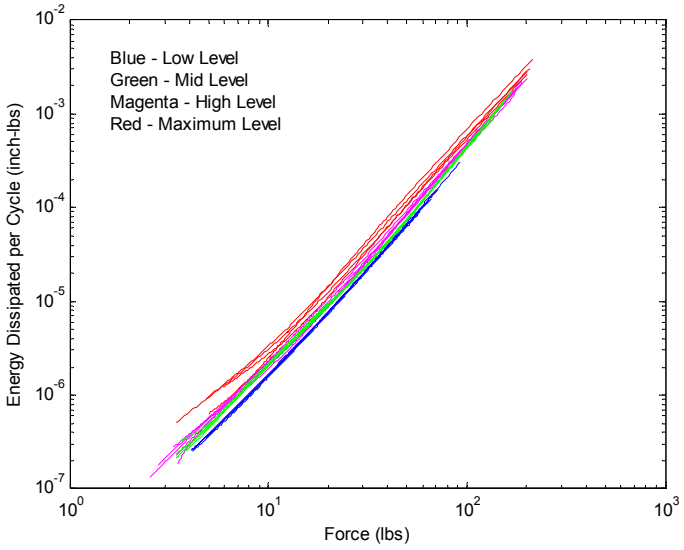

Figure 46. Energy dissipation curves for all jointed responses.

As was mentioned earlier, problems arise when the hammer forces are high enough to provide significant excitation to the bending mode of the system. Not only does the bending tend to modulate the decay of the responses creating problems in fitting the envelope to the peaks, but also the bending is likely responsible for generating some additional damping in the joint that is not present during lower levels of excitation. Therefore, the curves for the maximum levels of excitation in Figure 46 tend to indicate higher damping.

The quality of responses for more modest excitation levels is still very good. Figure 47 is a plot of energy curves for low, mid, and high levels of hammer impacts along with energy dissipation data points from steady state sine vibration testing. All the curves show fairly good agreement with each other. Also, the curves indicate that the energy dissipation in the transient experiment is slightly higher than energy dissipation measured in steady state experiments. As discussed later, the differences in the computed energy dissipation between the steady state and transient experiments are likely created by the different boundary conditions for the two experimental configurations.

Notice that the energy dissipation curves in Figure 47 have been truncated to display only the dissipation data corresponding to force amplitudes above 20 pounds. In these experiments, below 20 pounds, the energy dissipation that is measured is likely corrupted by various mechanisms. First, the signal-to-noise ratio of the response that is measured decreases at lower amplitudes. Second, the polynomial fit of the log of the peaks in the response contains artifacts that are more pronounced toward the end of the fit (lowest amplitudes), causing artificial fluctuations in the calculated damping. Lastly, in this experiment the dynamics of the seismic mass enter into the boundary condition and are probably more influential on the response at low amplitudes. Figure 48 shows the linear fit of the energy dissipation data above 20 pounds of force. Note that a straight line fit over the whole force range would yield a line of different slope that would not be as representative of the joint behavior.

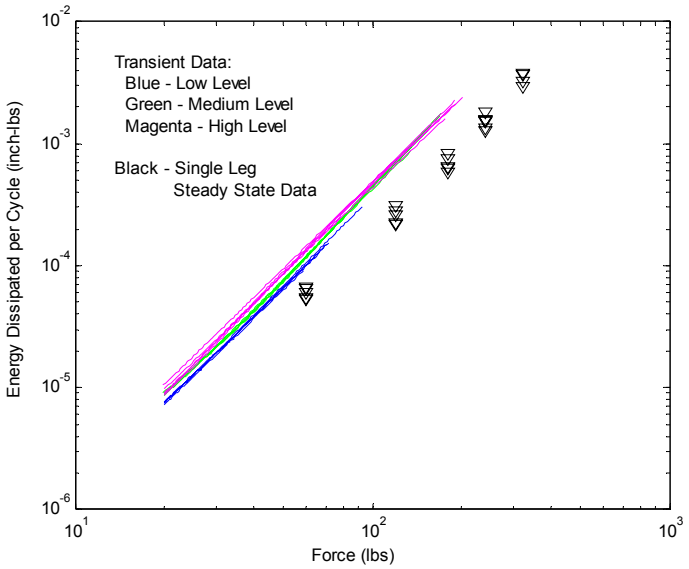

Figure 47. Transient and steady state energy dissipation.

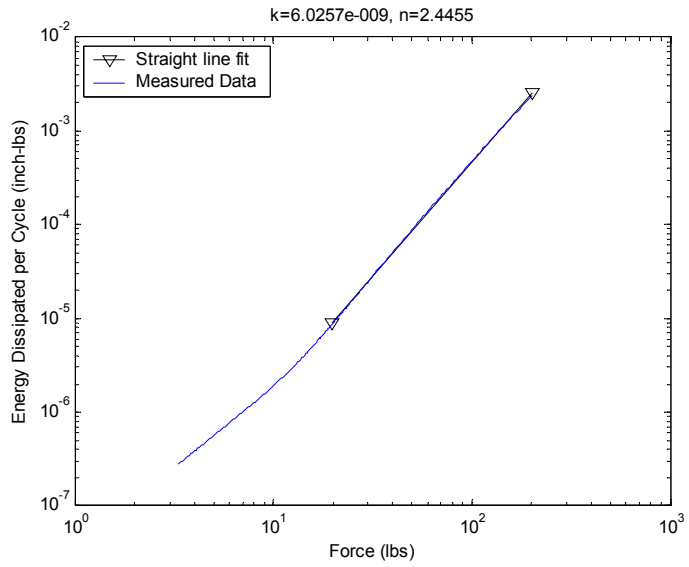

Figure 48. Linear fit of energy dissipation data above 20 lbs for a jointed single leg specimen.

A similar set of experiments was performed with the solid single leg inserted into the same experimental setup as used for the jointed single leg. These experiments were performed to establish a baseline for other energy losses in the experimental setup including the seismic mass. The response of the solid leg was recorded at various excitation levels. Unlike the jointed responses, the responses for the solid leg without the variability introduced by the joint were very repeatable. Figure 49 shows energy dissipation versus force behavior for the solid leg in both the transient and steady state experiments. The results, as in the case for the jointed single leg, indicate that the energy dissipated is higher for the transient experiment than for the sinusoidal experiments. Because there is no bolted joint available

to dissipate energy, the difference in the sinusoidal and transient results are an indication that there are other mechanisms of energy loss available in the transient experiment. It is likely that the transient response of the seismic mass to the hammer impact also dissipates energy in addition to the energy dissipated within the bolted joint.

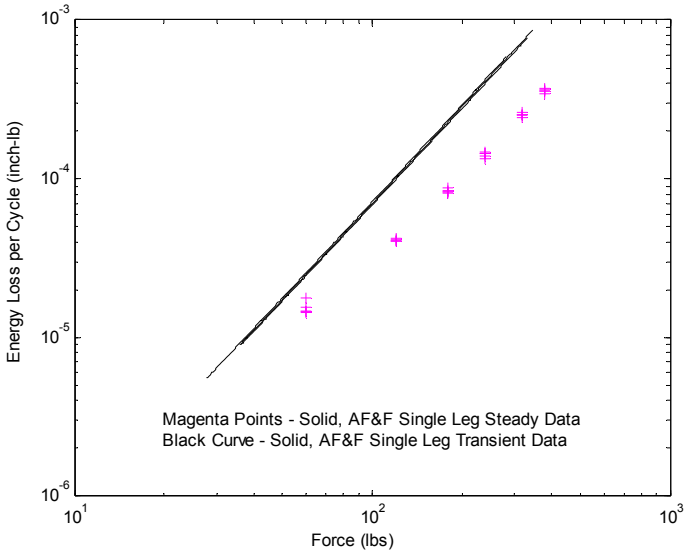

Figure 49. Solid single leg energy curves – transient vs. steady state.

For a solid leg that contains only linear damping, the slope of the curve on a log-log plot should be exactly 2.0. Figure 50 shows a straight line fit of a solid leg energy curve. The slope of 2.02 does indicate nearly linear damping.

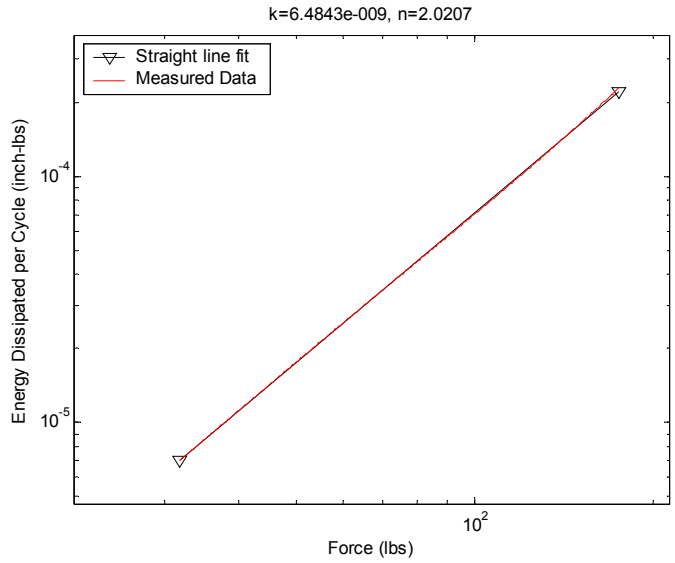

Figure 50. Solid specimen energy curve and straight line fit with slope = 2.02

The amplitudes and slopes on a log-log plot of the energy dissipated versus force curves for the jointed structure were calculated for all the useful data (not including the maximum excitation level containing large bending effects). Figure 51 show the slopes of straight-line fits of the curves for internal loads above 20 lbs. Notice that the calculated slope mean and standard deviation are very close to those values that were given earlier for steady state sine vibration data (mean of 2.429 and standard deviation of 0.05218).

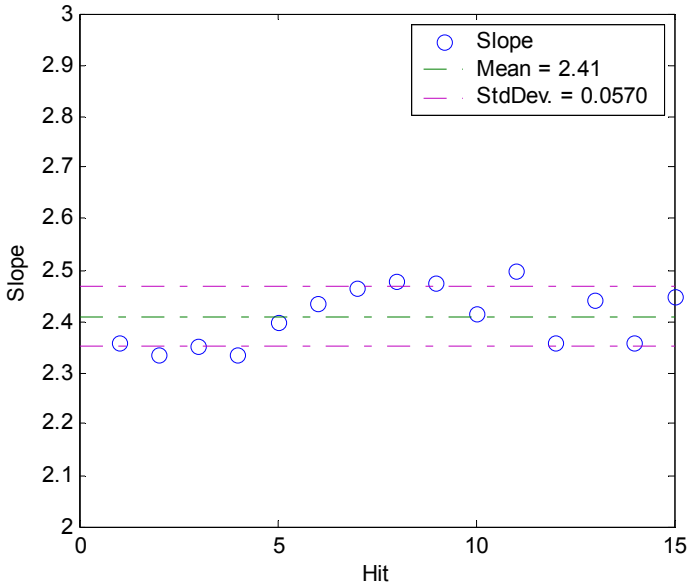

Figure 51. Single leg energy curve slopes for internal forces levels above 20 lbs.

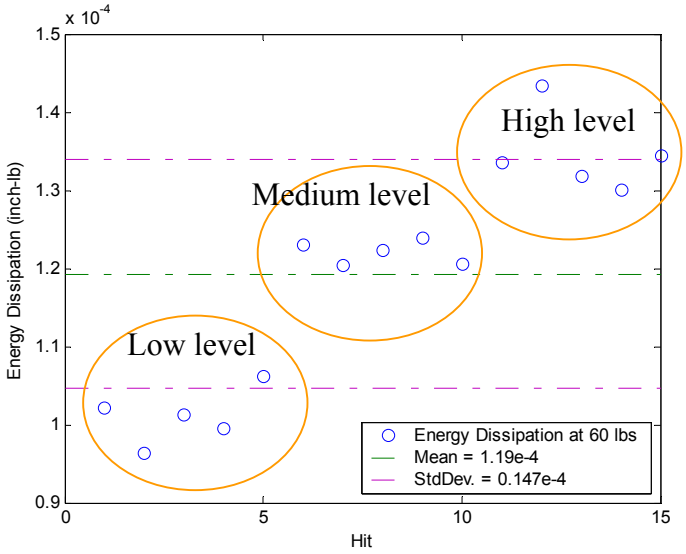

Figure 52. Energy dissipation at 60 lbs for low, medium and high level hits.

Figure 52 shows the amplitudes of each straight-line fit computed at 60 pounds of internal force for three levels of hammer impact level. There appears to be a dependence of energy dissipation on initial excitation level as shown Figure 52. Earlier, it was suggested that the effects of the bending mode were not as pronounced during the more moderate hammer inputs as there were during the very highest hammer inputs (nearly 700 lbs peak force). However, it is appears that the bending effects still contribute a the lower levels. As the hammer excitation is increased the bending action in the joint appears to dissipate more energy than just that associated with the single axial mode alone.

Scaling Energy Curves According to Steady State Data

Figure 47 and Figure 49 show that there is small disagreement in the energy dissipation between the solid specimens when measured using steady state sine testing and transient ring-down testing. It makes sense that the solid specimen should dissipate the same amount of energy in any configuration. However, there are differences between the transient and the steady state experiments in the boundary conditions. In the steady state experiment, the hardware is mounted directly to the shaker head, and the base motion of the experiment is enforced by the vibration control system regardless of the dynamics of the experiment. The transient experiment was performed on a very large seismic mass that would tend to provide mechanisms for additional energy dissipation. Also, in order to mount the single leg experiment to the seismic mass, additional holes had to be drilled in the base of the single leg mount, causing unknown changes in the dynamic behavior of the hardware. However, one would still expect that the addition of a bolted joint in the experiment would still show the same increase in energy dissipation over the solid unit in the transient experiment as it did in the steady experiment. To illustrate this theory, the energy curve in Figure 49 was scaled by a factor of 0.35 in order to make it line up with the steady data as seen in Figure 53.

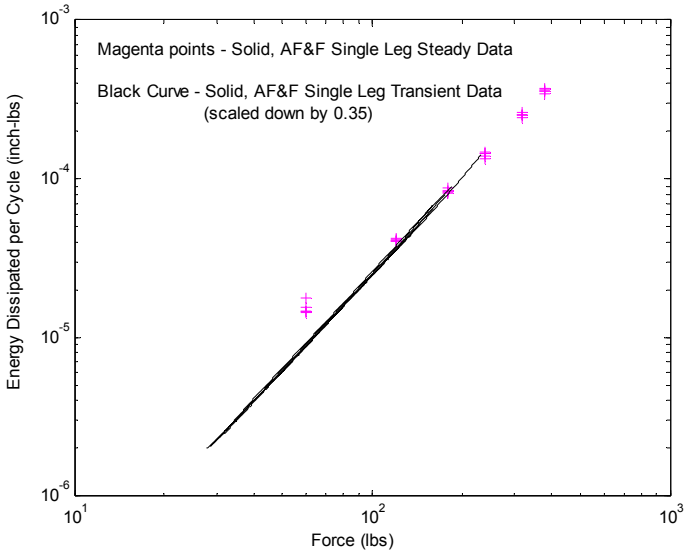

Figure 53. A scaling factor of 0.35 applied to the transient energy dissipation curves in order to make them coincide with steady state data.

The result of applying the same scaling factor to the jointed data from the transient experiment is seen in Figure 54. Now both the transient and steady data tend to agree for both solid and jointed specimens. It is likely that the raw measured energy dissipation for the transient experiments was consistently high due only to differences in boundary conditions from those of the steady state experiment.

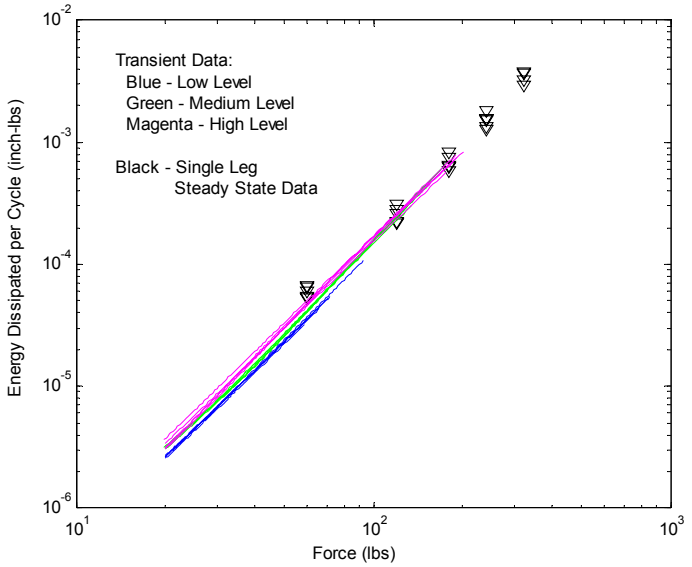

Figure 54. Transient dissipation curves in good agreement with steady state energy dissipation measurements after scaling by a factor of 0.35.

The transient ring-down technique for obtaining energy dissipation curves of single degree of freedom systems appears to be efficient and accurate. The technique is designed to estimate the nonlinear damping of a single mode of transient response as it decays. In most bolted joints experiments, the dynamics of the simple hardware are controlled in a way that usually ensures a simple response containing only one mode. However, when more complex structures containing many modes are tested, it is hard to excite the structure in a way that only one mode dominates the response. In those cases, a different technique for obtaining damping versus amplitude may need to be employed.

Conclusion

The experimental results presented here provide both insight and quantitative information about the dynamics of the bolted connection of the AF&F. Multiple sinusoidal experiments were performed, and the energy dissipation vs. force curves were calculated based on measured responses. The energy dissipation curves demonstrated the anticipated power-law relationship with amplitudes characteristic of mechanical joints undergoing microslip. The multiple sets of data collected after making and breaking the bolted joint provided data to evaluate the variability of the joint. The results show that the slope of the energy dissipation curve varied only slightly about the mean while the overall amplitude of

each energy curve varied from 20 to 30 percent. The effect of closing the vertical gap created a small increase in energy dissipation and slightly more variation in the results.

The solid leg proved to be very valuable in assessing the energy loss associated with the bolted joint. The energy dissipated in the solid leg was much less than the energy dissipated in the bolted joint, and it served as a reference to compare the jointed data. The solid leg represents a nearly linear system, and allowed for other losses in the experiment to be quantified, and provides a means for the jointed connection data to be adjusted for these losses.

A technique was demonstrated to compute energy dissipation curves from transient response data. This technique holds promise as an efficient means of obtaining energy dissipation measurements for jointed interface experiments. Problems with the technique can occur when adjacent vibration modes combine with the desired modal response to create a beating effect. Multi-degree-of-freedom techniques will be explored in the future.

The hammer impact tests with the experimental system attached to the large seismic mass suffer from two uncontrolled effects. The first is that the seismic mass represents another part of the combined system, has its own dynamics, and provides additional avenues of energy loss that are difficult to separate from the desired loss in the joint. The second is that the off-centered application of the impact excites a bending mode that is not present in the shaker tests. The unknown energy losses in the system are estimated from the solid leg data and used to adjust the results obtained from the jointed leg experiments. The effect of the bending mode could partially be accounted for by using the internal force gage data that tended to null the bending response in the signal such that more accurate curve fitting of the peaks could be accomplished. The bending action in the joint still provides a prying action and changes the contact pressure within the joint that will alter the microslip and ultimately the energy dissipation. The data suggest that this effect increases along with the energy dissipation with impact level. Even with these issues, good comparison was achieved between sinusoidal and the adjusted transient data.

These experimental efforts provide the results to perform analytical model correlation and ultimately validation by using one type of excitation, such as sinusoidal, to develop parameters for a joint model (calibration) and then use a second type of loading to provide a set of data to compare the model prediction (correlation/validation). Future efforts will address shaker driven shock excitations to provide complex shock waveforms characteristic of normal and high-level shock loads.

References

1. D. J. Segalman, *An Initial Overview of Iwan Modeling for Mechanical Joints*, SAND2001-0811, Sandia National Laboratories, Albuquerque, NM, March 2001.

2. D. J. Segalman, *A Four Parameter Iwan Model for Lap-Type Joints*, SAND2002-3828, Sandia National Laboratories, Albuquerque, NM, November 2002.

3. D. O. Smallwood, D. L. Gregory, and R. G. Coleman, A Three Parameter Constitutive Model for a Joint which Exhibits a Power Law Relationship Between Energy Loss and Relative Displacement, *72nd Shock and Vibration Symposium, Destin FL, Nov. 2001.*

4. D. L. Gregory, D. O. Smallwood, R. G. Coleman, and M. A. Nusser, Experimental Studies to Investigate Damping in Frictional Shear Joints, *70th Shock and Vibration Symposium, NM, Nov. 1999.*

5. D. O. Smallwood, D. L. Gregory, and R. G. Coleman, Damping Investigations of a Simplified Frictional Shear Joint, *71st Shock and Vibration Symposium, Arlington, VA, Nov. 2000*.

6. Harris, C. M. *Shock and Vibration Handbook*, 4th edition, Eq. 2.41, McGraw-Hill, New York, NY, 1996.

7. ABAQUS/Standard Users Manual Version 5.8-1, Hibbitt, Karlsson & Sorensen, Inc., Pawtucket, RI, 1999.

8. Thomson, W. T., *Vibration Theory and Applications*, Prentice-Hall, Englewood Cliffs, NJ, 1965.

Distribution:

1 University of Illinois
Attn: Prof. Lawrence A. Bergman
306 Talbot Lab
104 S. Wright St.
Urbana, IL 61801

1 Los Alamos National Laboratory
Attn: Dr. Scott Doebling, MS P946
P.O. Box 1663
Los Alamos, NM 87545

1 University of New Mexico
Attn: Professor Larissa Gorbatikh
MSC 011150
Mechanical Engineering Building
Albuquerque, NM 87131

1 Los Alamos National Laboratories
Attn: Norman F. Hunter, MS C931
ESA-MT
Los Alamos, NM 87545

1 University of Akron
Attn: Prof. D. Dane Quinn
Department of Mechanical Engineering
107b Auburn Science and Engineering Center
Akron, OH 44325-3903

1 University of New Mexico
Attn: Professor Henry Schreyer
MSC 011150
Engineering Mechanical Building
Albuquerque, NM 87131

1 MS0553 Bateman, V.I., 9126
1 MS0555 Garrett, M.S., 9122
10 MS0555 Gregory, D.L., 9122
5 MS0555 Resor, B.R., 9122
1 MS0555 Stasiunas, E. C, 9124
1 MS0557 Baca, T. J., 9125
1 MS0557 Carne, T.G., 9124
1 MS1135 Coleman, R.G., 9122
1 MS0557 Epp, D. S., 9125
1 MS0557 Mayes, R. L., 9125
1 MS0557 O'Gorman, C., 9125
1 MS0557 Paez, T. L., 9133
1 MS0557 Simmermacher, T. W, 9124
1 MS0557 Sumali, H., 9124
1 MS0557 Urbina, A., 9133
1 MS0824 Moya, J. L., 9130
1 MS0824 Ratzel, A. C., 9110
1 MS0828 Pilch, M., 9133
1 MS0834 Johannes, J. E., 9114
1 MS0835 Alvin, K. F., 9142
1 MS0835 McGlaun, J. M., 9140
1 MS0841 Bickel, T. C., 9100
1 MS0847 Adams, C., 9125
1 MS0847 Attaway, S. W., 9134
1 MS0847 Bhardwaj, M. K., 9142
1 MS0847 Bitsie, F., 9124
1 MS0847 Dohrmann, C. R., 9124
1 MS0847 Fulcher, C. W. G., 9125
1 MS0847 Heinstein, M. W, 9142
1 MS0847 Hinnerichs, T., 9126
1 MS0847 Hopkins, R. N., 9125
1 MS0847 Jung, J., 9127
1 MS0847 May, R. A., 9126
1 MS0847 Mitchell, J. A., 9142
1 MS0847 Morgan, H. S., 9120
1 MS0847 Ozdoganlar, O. B., 9124
1 MS0847 Red-Horse, J. R., 9133
1 MS0847 Redmond, J. M., 9124
1 MS0847 Reese, G. M., 9142
1 MS0847 Segalman, D. J., 9124
1 MS0847 Starr, M. J., 9124
1 MS0847 Walther, H. P., 9125
1 MS0847 Wojtkiewicz, S., 9124
1 MS1393 Chu, T. Y., 9100

1 MS9018 Central Technical Files, 8945-1
2 MS0899 Technical Library, 9619
1 MS0612 Review & Approval Desk, 9612